Chem Soc Rev

REVIEW ARTICLE

Earth-abundant cocatalysts for semiconductor-based photocatalytic water splitting

Cite this: DOI: 10.1039/c3cs60425j

Jingrun Ran,[a] Jun Zhang,[ab] Jiaguo Yu,[b] Mietek Jaroniec[c] and Shi Zhang Qiao*[a]

Received 23rd November 2013

DOI: 10.1039/c3cs60425j

www.rsc.org/csr

Photocatalytic water splitting represents a promising strategy for clean, low-cost, and environmental-friendly production of H_2 by utilizing solar energy. There are three crucial steps for the photocatalytic water splitting reaction: solar light harvesting, charge separation and transportation, and the catalytic H_2 and O_2 evolution reactions. While significant achievement has been made in optimizing the first two steps in the photocatalytic process, much less efforts have been put into improving the efficiency of the third step, which demands the utilization of cocatalysts. To date, cocatalysts based on rare and expensive noble metals are still required for achieving reasonable activity in most semiconductor-based photocatalytic systems, which seriously restricts their large-scale application. Therefore, seeking cheap, earth-abundant and high-performance cocatalysts is indispensable to achieve cost-effective and highly efficient photocatalytic water splitting. This review for the first time summarizes all the developed earth-abundant cocatalysts for photocatalytic H_2- and O_2-production half reactions as well as overall water splitting. The roles and functional mechanism of the cocatalysts are discussed in detail. Finally, this review is concluded with a summary, and remarks on some challenges and perspectives in this emerging area of research.

1. Introduction

The global energy supply and related environmental issues are among the biggest technological challenges being confronted by chemists and technologists in the 21st century. The rate of worldwide energy consumption reached 15 TW in 2008 and is expected to nearly double by 2050 due to the growing global production and population.[1] In contrast, our major energy resources still originate from limited and non-renewable fossil

[a] School of Chemical Engineering, The University of Adelaide, Adelaide, SA 5005, Australia. E-mail: s.qiao@adelaide.edu.au
[b] State Key Laboratory of Advanced Technology for Material Synthesis and Processing, Wuhan University of Technology, Wuhan, 430070, P. R. China
[c] Department of Chemistry and Biochemistry, Kent State University, Kent, Ohio 44242, USA

Jingrun Ran

Jingrun Ran received his BE and ME degrees in Materials Science and Engineering from the Wuhan University of Technology in 2009 and 2012, respectively. He is currently a PhD candidate in Chemical Engineering under the supervision of Professor Shi Zhang Qiao at the University of Adelaide. His current research is focused on the development of novel nano-structured photocatalysts and photoelectrodes for solar-light-driven water splitting.

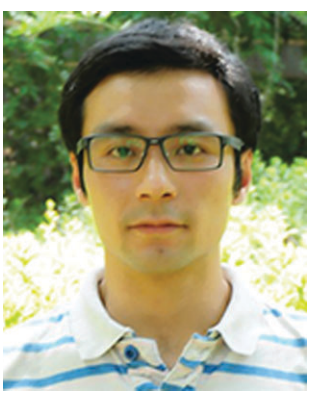

Jun Zhang

Jun Zhang received his PhD in Materials Physics and Chemistry in 2010 from the Wuhan University of Technology. Later he joined Prof. Jiaguo Yu's group as a research assistant professor at the State Key Laboratory of Advanced Technology for Materials Synthesis and Processing, Wuhan University of Technology. From 2012 to 2013, he was a visiting scholar in Prof. Shi Zhang Qiao's group at the University of Adelaide. His research interests include the design and fabrication of photocatalytic materials for energy and environmental applications.

fuels, such as coal, oil and natural gas. Furthermore, the combustion of these fossil fuels has caused a series of critical environmental problems, ranging from air and water contamination to global warming. Therefore, seeking renewable, clean and carbon-neutral alternative energy resources is urgently needed to limit our dependence on fossil fuels. Solar energy is widely accepted as a free, abundant and endlessly renewable source of clean energy, which could meet current and future human energy demand. Thus, the harvest and conversion of solar energy into a usable energy form is highly desirable.[2–4] Nowadays the most popular way to use solar energy is through photovoltaic cells, which could directly convert solar energy into electricity. However, the electricity must be used immediately or stored in a secondary device, such as capacitors and batteries. In comparison, the production of chemical fuels *via* photocatalytic processes represents a more attractive approach to harness solar energy, which could harvest and store solar energy in the form of molecular bonds through a thermodynamic uphill reaction.

Photocatalytic water splitting into hydrogen and oxygen using semiconductor photocatalysts has become a promising strategy for converting solar energy into clean and carbon-neutral H_2 fuel *via* a low-cost and environmentally benign route since Honda and Fujishima discovered the photoelectrochemical (PEC) water-splitting on a titania electrode in 1972.[5] In general, the overall photocatalytic water splitting reaction involves three major steps: (i) absorption of light by a semiconductor to generate electron–hole pairs, (ii) charge separation and migration to the surface of the semiconductor, and (iii) surface reactions for H_2 or O_2 evolution (Fig. 1). The overall

Jiaguo Yu

Jiaguo Yu received his BS and MS in chemistry from Huazhong Normal University and Xi'an Jiaotong University, respectively, and his PhD in Materials Science in 2000 from the Wuhan University of Technology. In 2000, he became a Professor of the Wuhan University of Technology. He was a post-doctor of the Chinese University of Hong Kong from 2001 to 2004, visiting scientist from 2005 to 2006 at the University of Bristol, and visiting scholar from 2007 to 2008 at the University of Texas at Austin. His research interests include semiconductor photocatalysis, photocatalytic hydrogen production, solar fuels, dye-sensitized solar cells, adsorption, CO_2 capture, graphene and so on.

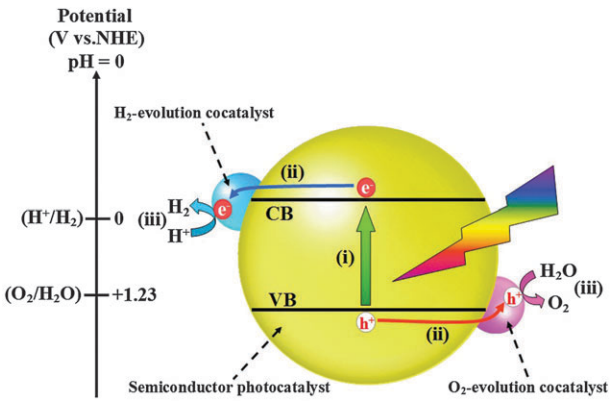

Fig. 1 Schematic illustration of photocatalytic water splitting over a semiconductor photocatalyst loaded with H_2- and O_2-evolution cocatalysts.

Mietek Jaroniec

Mietek Jaroniec received his MS and PhD from M. Curie-Sklodowska University, Poland, in 1972 and 1976, respectively. Since 1991 he is a Professor of Chemistry at Kent State University, Kent, Ohio (USA). Before joining Kent State he was a Professor of Chemistry at M. Curie-Sklodowska University, Poland. His research interests revolve primarily around interdisciplinary topics of interfacial chemistry, chemical separations, and chemistry of materials, including physical adsorption at the gas/solid and liquid/solid interfaces, gas and liquid chromatography, adsorbents and catalysts. At Kent State he has established a vigorous research program in the area of ordered nanoporous materials such as ordered mesoporous silicas, organosilicas, inorganic oxides and carbons, focusing on their synthesis and environmental and energy-related applications.

Shi Zhang Qiao

Prof. Shi Zhang Qiao received his PhD degree in chemical engineering from the Hong Kong University of Science and Technology in 2000, and is currently a professor (Chair of Nanotechnology) at the School of Chemical Engineering of the University of Adelaide, and an Honorary Professor at the University of Queensland, and an Associate Editor of Journal of Materials Chemistry A. His research expertise is in nanomaterials and nanoporous materials for drug/gene delivery and new energy technologies. He has been honoured with a prestigious ARC Discovery Outstanding Researcher Award (DORA, 2013), an Emerging Researcher Award (2013, ENFL Division of the American Chemical Society) and a UQ Foundation Research Excellence Award (2008).

efficiency of photocatalytic water splitting is determined by the balance of thermodynamics and kinetics of the above three steps altogether. In the past several decades, tremendous efforts have been devoted to developing photocatalysts with broader absorption of the solar energy spectrum (step i) as well as efficient charge separation and migration (step ii). For instance, a series of strategies have been employed to enhance the light absorption of wide-bandgap semiconductors, such as bandgap engineering (*e.g.* ion doping and forming solid solutions),[6–12] coupling with narrow-bandgap semiconductors,[13–16] dye sensitization,[17–19] surface plasmonic enhancement[20–22] and disorder engineering.[23,24] Besides, many novel single-phase semiconductors of narrow bandgap have also been developed, such as graphitic-C_3N_4[25] and Ag_3PO_4.[26] On the other hand, in order to gain efficient charge separation and transportation, various nanostructured semiconductors (*e.g.* nanoparticles, porous nanospheres, nanowires, nanobelts, nanotubes and nanosheets) designed with short charge diffusion length, high crystallinity and less defects have been fabricated.[27–34] Moreover, the formation of a semiconductor hetero-junction is also extensively applied to improve the charge separation and transfer.[35–39] Up till now, many reviews have been published to mainly summarize the achievement and progress in enhancing the efficiency of the first two steps in photocatalytic water splitting.[2,40–51] As shown in Fig. 1, the third step is promoted by the presence of a H_2-evolution or O_2-evolution cocatalyst, which could extract photogenerated charge carriers, host active sites for catalytic H_2 or O_2 evolution and improve the stability of photocatalysts by suppressing photo-corrosion. Therefore, cocatalysts play a significant role in improving both the activity and stability of semiconductor photocatalysts.

Currently, most of the developed photocatalyst systems utilize noble-metal-based cocatalysts to achieve high photocatalytic activity. For example, Ru,[52,53] Rh,[54,55] Pd,[56] Pt,[57–64] Au[64,65] and Ag[66,67] have been extensively investigated as efficient cocatalysts for photocatalytic hydrogen evolution. Among them, Pt is the most effective cocatalyst due to its largest work function and lowest overpotential for H_2 evolution.[68] The highest photocatalytic activities for hydrogen production using visible-light irradiation are from photocatalysts loaded with Pt as the cocatalyst.[28,61] On the other hand, noble metal oxides, such as RuO_2[69–71] and IrO_2,[72–74] are well-known as excellent water oxidation cocatalysts for improving the photocatalytic O_2-production activity. For overall water splitting, the backward reactions of H_2 and O_2 recombination together with photoreduction of O_2 must be suppressed. Therefore, cocatalysts with excellent activity and selectivity, which could both promote forward H_2 or O_2 evolution and inhibit the backward reactions, are essential for achieving high efficiency in photocatalytic pure water splitting. Up to now, the most active cocatalysts for assisting H_2 evolution in overall water splitting are $Rh_{2-y}Cr_yO_3$[75] and core–shell-structured Rh–Cr_2O_3.[55,76]

Unfortunately, the above noble-metal based cocatalysts are too scarce and expensive to be used for large-scale energy production. Therefore, the development of noble-metal free cocatalysts with high efficiency and low cost is highly desirable. In recent years, many kinds of novel cocatalysts constructed from cheap and earth-abundant elements have been developed for assisting photocatalytic water splitting. For example, $Cu(OH)_2$[77] and $Ni(OH)_2$ clusters[78–80] for the first time have been utilized as highly efficient cocatalysts for improving the photocatalytic activity of various semiconductors, *e.g.* TiO_2, CdS and g-C_3N_4. Nanocarbon materials, such as carbon nanotubes[81,82] and graphene nanosheets,[83–86] also demonstrated their strong capability to enhance the photocatalytic H_2-production activity as metal-free cocatalysts. Furthermore, the combination of graphene nanosheets with sheet-like MoS_2 formed a highly active composite cocatalyst, which greatly advanced the photocatalytic activity of TiO_2 promoted by synergetic effects.[87] Natural hydrogenases[88,89] and artificial molecules, such as hydrogenase mimics[90–92] and Ni complexes,[93,94] are proven to be high-efficiency H_2-evolution cocatalysts. A novel metal-free O_2-evolution cocatalyst, $B_2O_{3-x}N_x$ nanocluster, showed the capability of apparently improving the photocatalytic activity of WO_3.[95] Bio-inspired molecular cocatalysts, such as the $[Mo_3S_4]^{4+}$ cluster, were reported to be effective in photocatalytic overall water splitting.[96] Since many great achievements in earth-abundant cocatalysts have been made in recent years and there is still no review introducing them, we believe that a comprehensive review on this subject is timely to promote further developments in this important area of research. In this review, we will focus on all the earth-abundant cocatalysts developed to date for photocatalytic H_2- and O_2-evolution half reactions as well as overall water splitting. The roles and functional mechanism of cocatalysts in photocatalytic water splitting will be discussed and summarized.

2. Fundamentals of cocatalysts in photocatalytic water splitting

2.1 Roles of cocatalysts in photocatalytic water splitting

In photocatalytic water splitting, the H_2- and O_2-evolution cocatalysts play three different pivotal roles for improving both the activity and reliability of semiconductor photocatalysts:

(i) Cocatalysts could lower the activation energy or overpotential for H_2- or O_2-evolution reactions on the surface of semiconductors. The O_2-evolution reaction is a four-electron transfer process coupled to the removal of four protons from water molecules to form an oxygen–oxygen bond. Therefore, this half reaction is regarded as the greatest challenging step in the photocatalytic water splitting. Thus, the utilization of cocatalysts with low O_2-evolution overpotential could notably boost the efficiency of photocatalytic O_2-evolution reactions.

(ii) Cocatalysts are capable of assisting in electron–hole separation at the cocatalyst/semiconductor interface. As displayed in Fig. 1, the photogenerated electrons on the conduction band (CB) of a photocatalyst are transferred to the H_2-evolution cocatalyst and reduce protons to H_2 molecules, whereas photogenerated holes on the valence band (VB) of this photocatalyst migrate to the O_2-evolution cocatalyst and oxidize H_2O to form O_2. The formation of an appropriate hetero-junction

between the cocatalyst and the semiconductor is the key factor for promoting the charge separation and transfer from the semiconductor to the cocatalyst. Firstly, the relative energy level at the hetero-junction interface dictates the direction and efficiency of the carrier separation and transportation. Secondly, the heterostructure with a short distance between the semiconductor and the cocatalyst can reduce the necessary charge transfer distance, effectively inhibiting the bulk recombination and enhancing the overall efficiency.

(iii) Cocatalysts could suppress the photo-corrosion and increase the stability of semiconductor photocatalysts. For instance, many visible-light-responsive semiconductors, such as (oxy)sulfides[12,16,22,27,28,37,52,60,61,79,81–83,85,88,97–99] and (oxy)-nitrides,[25,69,75,76,80,100–106] are susceptible to oxidation by photogenerated holes, resulting in their self-decomposition. The loading of cocatalysts on these semiconductors could inhibit their decomposition by extracting the photogenerated holes for O_2 evolution, thus enhancing the robustness of semiconductors.

2.2 Factors influencing the performance of cocatalysts

Many factors can affect the capability of H_2- and O_2-evolution cocatalysts in the semiconductor-based photocatalytic water splitting, such as the cocatalyst loading amount, its particle size and structure. As demonstrated in Fig. 2, there is a volcano-type trend between the loading amount of a given cocatalyst and the photocatalytic activity (regardless of the synthesis method, photocatalyst type and loaded cocatalyst). Initially, the introduction of a cocatalyst onto a semiconductor could gradually enhance the photocatalytic water splitting activity by facilitating charge collection and gas evolution reactions. When the loading amount of a cocatalyst on a semiconductor reaches the optimal value, this cocatalyst/semiconductor system achieves the highest activity. However, further loading of the cocatalyst will drastically decrease the photocatalytic activity. This decrease is caused by the following factors: (i) high cocatalyst loading amount that could result in covering the surface active sites of the semiconductor and hindering its contact with sacrificial reagents or water molecules; (ii) excessive loading of cocatalysts on the surface of semiconductors that could shield the incident light, and thus prevent the light absorption and generation of photogenerated electrons and holes inside the semiconductor; (iii) large particle size deteriorates the catalytic properties of cocatalysts or leads to the disappearance of surface effects; and (iv) cocatalysts at high loading amount could act as charge recombination centers, resulting in the decrease of the photocatalytic activity. This phenomenon is widely observed in the cocatalyst/semiconductor photocatalyst systems.

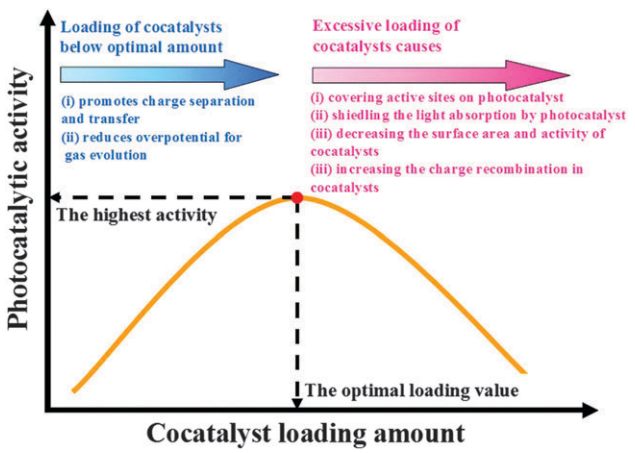

Q3 Fig. 2 A volcano-type relationship between the loading amount of a cocatalyst and the photocatalytic activity of the cocatalyst-loaded semiconductor photocatalyst.

Another important factor influencing the catalytic activity of cocatalysts is their size. Normally, at the same loading amount, cocatalysts with smaller size have a larger surface area and more active sites, which result in higher catalytic activity. In addition, the charge carriers are less likely to recombine in the bulk of small particles of a cocatalyst than in the large ones. In some cases, smaller particles of cocatalysts may exhibit lower barriers for the interfacial charge transfer from semiconductors to cocatalysts (*e.g.* electron-tunneling effect). In fact, numerous studies show that the small size and high dispersion of the loaded cocatalysts lead to significantly enhanced photocatalytic efficiency.[64,77,78,96,100,107–126] Furthermore, artificial molecular cocatalysts with very small dimensions like $[Mo_3S_4]^{4+}$ are composed of surface atoms/edge sites only and possess an optimized number of active sites, which could substantially increase the photocatalytic activity of semiconductors.[96] For some cocatalysts, such as the well-known core–shell Ni–NiO (NiO_x)[35,117,119,120,127–136] and Rh–Cr_2O_3 (ref. 76, 103 and 126) particles, their structure plays an important role in achieving the high activity for overall photocatalytic water splitting. The shell of these core–shell structures could suppress the reverse reaction of H_2 and O_2 as well as photoreduction of O_2, protect the metal core from corrosion and improve the robustness of cocatalysts. The knowledge of this type of structures would be beneficial for the design and fabrication of other efficient and stable cocatalysts for photocatalytic water splitting.

3. Earth-abundant cocatalysts for photocatalytic H_2-evolution half reactions

3.1 Transition metal cocatalysts for H_2 evolution

In addition to rare and expensive noble metals, some earth-abundant and low-cost transitional metals, such as Co,[124] Ni[66,67,107,108,117,124,125,137,138] and Cu,[64,67,139,140] have also been applied as cocatalysts in photocatalytic H_2 production. The loading of these metals on semiconductors results in the formation of a Schottky barrier at the metal/semiconductor interface. The Schottky barrier is a kind of junction, which could promote charge separation. On the other hand, these metals (*i.e.* Co, Ni and Cu) are capable of catalyzing the proton reduction to H_2 molecules. Therefore, an enhanced photocatalytic H_2 production activity could be observed when these metals are loaded as cocatalysts on semiconductors.

In general, three different methods, including *in situ* photoreduction,[66,67,108,125,138] chemical reduction[107,124] and impregnation-calcination/reduction methods,[64,117,137,139,140] have been employed to load these metals as clusters/nanoparticles (NPs) on semiconductors. Wu *et al.*[139] have deposited Cu NPs on TiO_2 by incipient-wetness impregnation followed by calcination/reduction. The photocatalytic H_2-production activity of Cu-loaded TiO_2 exhibited a 10-fold enhancement at the optimum loading of ~1.2 wt% Cu. In contrast, the doping of Cu ions into TiO_2 lattice resulted in a lower photocatalytic activity. Lin *et al.*[64] reported that the production rate of H_2 on Cu-loaded mesoporous Nb_2O_5 is about 5 times faster than that of pure mesoporous Nb_2O_5. Foo and coworkers[140] studied the photocatalytic activity of TiO_2 loaded with Cu–Cu_2O core–shell NPs. They found that the Cu_2O shell would be rapidly reduced to metallic Cu by accepting electrons generated in TiO_2 under UV irradiation. The resulting Cu NPs could markedly increase the photocatalytic H_2-production rate of TiO_2 by a factor of 6. Korzhak *et al.*[66] showed that Cu-loaded TiO_2 has higher photocatalytic H_2-production activity than Ni-loaded TiO_2 due to the stronger electronic interaction between Cu NPs and TiO_2. Moreover, metallic Ni has also been widely employed as a H_2-evolution cocatalyst. The work by Husin *et al.*[117] shows that Ni is a more active cocatalyst than core shell Ni–NiO and NiO when loaded on $La_{0.02}Na_{0.98}TaO_3$ for hydrogen production, suggesting that the loading of metallic Ni with a high electrical conductivity is important in trapping and transferring electrons in photocatalytic reactions. Ultrafine Ni and NiO NPs (2 to 3 nm) were uniformly loaded on a graphene oxide (GO) sheet using a simple chemical reduction method. The photocatalytic hydrogen production activity from aqueous methanol solution was enhanced, approximately 4-fold for NiO–GO and 7-fold for Ni–GO, compared to bare GO.[107] Yu *et al.*[108] reported that Ni-loaded TiO_2 exhibited a H_2-production rate of 2547 μmol h^{-1} g^{-1} with a quantum efficiency (QE) of 8.1% at 365 nm, exceeding that of pure TiO_2 by 135 times. Moreover, Co- or Ni-decorated TiO_2 exhibited only three times lower photocatalytic H_2-production activities in comparison to Pt-decorated TiO_2, demonstrating that Co and Ni clusters are attractive alternatives to noble-metal Pt as H_2-evolution cocatalysts.[124] Dinh *et al.*[125] showed that the presence of Ni clusters as a cocatalyst could increase the photocatalytic H_2-production rate of the CdS–titanate nanocomposite by a factor of 77, reaching 11 038 μmol h^{-1} g^{-1}, corresponding to a QE of 21% at 420 nm. Very recently, Yamada *et al.*[109] found that Ni NPs with a smaller size displayed higher catalytic activity due to their larger specific surface area and more active sites. Also, hexagonally close-packed (hcp) Ni NPs were more catalytically active than face-centered-cubic (fcc) Ni NPs of similar size because the loose atomic packing of the hcp structure could offer enough space to accommodate a proton or hydrogen atom.[141]

It is well-known that the cheap and earth-abundant metals (*e.g.* Co, Ni and Cu) in bulk form require a higher overpotential for proton reduction in comparison to noble-metal Pt. However, the aforementioned results clearly show that these metals in the form of nanoparticles could tremendously enhance their relative catalytic activity in comparison to Pt as a cocatalyst in photocatalytic H_2 production. This enhancement can be attributed to the improvement of intrinsic electrocatalytic activities of Co, Ni and Cu cocatalysts at the nanoscale level because of the significant increase in the number of catalytic active sites due to an enlarged surface area, and stronger interfacial interactions, which lead to more efficient electron transfer from the semiconductor to the cocatalyst. Furthermore, the price of these earth-abundant metals is at least three orders of magnitude lower than that of Pt, which is a great advantage in practical applications. Therefore, Co, Ni and Cu NPs are promising candidates for replacing noble-metal Pt as cocatalysts in photocatalytic H_2 production.

3.2 Transition metal compounds as cocatalysts for H_2 evolution

3.2.1 Transition metal oxides and hydroxides. Several transition metal oxides, such as NiO,[107,110] NiO_x,[131,142–144] CuO[111,114,115,145–148] and Cu_2O,[148] are well-known as noble-metal-free cocatalysts for photocatalytic H_2 production. Sreethawong *et al.*[110] showed that NiO-loaded TiO_2 prepared by a single-step sol–gel (SSSG) method showed higher photocatalytic H_2-production efficiency than that prepared by an incipient wetness impregnation (IWI) method. The major reason of better photocatalytic H_2-production activity in the case of the NiO–TiO_2 catalyst prepared by the SSSG method is higher uniformity and dispersion of NiO NPs on TiO_2, which result in stronger interactions and thus, more efficient electron transfer. Generally, a suitable reduction–reoxidation pretreatment could significantly improve the activity of NiO as a cocatalyst on semiconductors for photocatalytic H_2 production.[142–144] The aforementioned pretreatment can be used to produce Ni–NiO core–shell structures, in which the metallic Ni core promotes the electron transfer from the semiconductor to the NiO shell. Tian *et al.*[142] investigated the incorporation of NiO, NiO_x, Pt and RuO_2 as cocatalysts on $K_4Ce_2Ta_{10}O_{30}$ photocatalyst for H_2 evolution under visible-light irradiation. The amount of H_2 evolved during 4 h on NiO_x-loaded $K_4Ce_2Ta_{10}O_{30}$ reached 135 μmol, which is about four times that on this photocatalyst co-loaded with Pt and RuO_2 and five times that on the same photocatalyst loaded with NiO. Choi and coworkers[143] reported that NiO_x–$KNbO_3$–CdS nanocomposite photocatalyst exhibited a three times higher visible-light photocatalytic H_2-production rate than $KNbO_3$–CdS, due to the deposition of NiO_x cocatalyst having active sites facilitating H_2 production. They also found that NiO_x is a much more active and stable cocatalyst than NiO on $KNbO_3$–CdS.

Apart from NiO and NiO_x, other metal oxide cocatalysts such as CuO and Cu_2O have also been proven to be beneficial for photocatalytic H_2 production. For example, Sreethawong *et al.*[145] reported that CuO-loaded TiO_2 displayed almost two times higher photocatalytic H_2-production activity than NiO-loaded TiO_2. Bandara *et al.*[146] fabricated highly stable CuO-loaded TiO_2 for photocatalytic H_2 production in methanol aqueous solution. They found that the photogenerated electrons in the CB of both TiO_2 and CuO accumulated to build up an excess of

electrons in the CB of CuO, which resulted in a negative shift in the Fermi level of CuO, and in the overpotential necessary for efficient H_2 production over CuO/TiO_2 photocatalyst. Xu *et al.*[147] reported that the as-prepared CuO/TiO_2 exhibited a photocatalytic H_2-production rate of 18 500 μmol h^{-1} g^{-1} in methanol aqueous solution, which is even higher than that of some Pt- or Pd-loaded TiO_2. Although the long-time irradiation caused the reduction of CuO and copper leaching in CuO–TiO_2, which decreased its photocatalytic activity to a certain degree, the activity could be partially recovered *via* a facile calcination procedure, which regenerated CuO deposited on TiO_2. Furthermore, they found that different chemical states of Cu species (Cu, Cu_2O and CuO) and their distribution ratio between the surface and the bulk phase of TiO_2 notably influenced the photocatalytic H_2-production activities.[148] Cu_2O showed the greatest enhancement in terms of initial H_2-production rate, followed by CuO, while the enhancement effect of metallic Cu was the lowest. They also found that Cu species on the surface of TiO_2 promote charge transfer more efficiently than those in TiO_2 lattice. However, Cu species in TiO_2 lattice showed better stability due to the restriction of Cu leaching. The work by Yu *et al.*[111] showed that the quantum-size effect of CuO clusters loaded on TiO_2 could modify the energy levels of the CB and VB edges of TiO_2 in the CuO–TiO_2 semiconductor system, which facilitates the electron transfer and improves the photocatalytic activity. Very recently, an especially high photocatalytic H_2-evolution rate of 99 823 μmol h^{-1} g^{-1} was achieved on CuO/TiO_2 photocatalyst in a water–glycerol mixture under natural sunlight irradiation, mainly due to the quantum-size effect of CuO cocatalyst, implying a bright future for large-scale solar photocatalytic water splitting using cheap and efficient photocatalysts.[115]

Recently, $Cu(OH)_2$,[77,116,149] $Ni(OH)_2$[78–80,150,151] and $Co(OH)_2$[152] have been developed as efficient and low-cost cocatalysts for photocatalytic H_2 production. Yu and coworkers[77] fabricated $Cu(OH)_2$ cluster-modified TiO_2 by a simple precipitation approach using Degussa P25 TiO_2 powder as a support and $Cu(NO_3)_2$ as a precursor (Fig. 3a). They found that $Cu(OH)_2$ content in the $Cu(OH)_2$–TiO_2 composite significantly influenced its photocatalytic H_2-evolution activity in ethylene glycol aqueous solution under irradiation with ultraviolet light emitting diodes (UV-LEDs) (Fig. 3b). The optimal $Cu(OH)_2$ loading amount was determined to be 0.29 mol%, resulting in a H_2-evolution rate of 3418 μmol h^{-1} g^{-1} with a QE of 13.9%, which exceeded the rate on bare TiO_2 by more than 205 times. As shown in Fig. 3c and d, the enhanced mechanism was observed because the potential of $Cu(OH)_2$/Cu ($Cu(OH)_2 + 2e^- = Cu + 2OH^-$, E^o = −0.224 V) was slightly lower than the CB (−0.26 V) of anatase TiO_2, which promotes the electron transfer from the CB of TiO_2 to $Cu(OH)_2$ clusters, forming Cu/$Cu(OH)_2$ clusters. These Cu/$Cu(OH)_2$ clusters can serve as a cocatalyst to facilitate the separation and transport of photoinduced electrons from TiO_2 to Cu/$Cu(OH)_2$ clusters, where H^+ is reduced to H_2 molecules. The major reaction steps in this photocatalytic process are summarized as eqn (1) and (2):

$$Cu(OH)_2 + 2e^- = Cu + 2OH^- \quad (1)$$

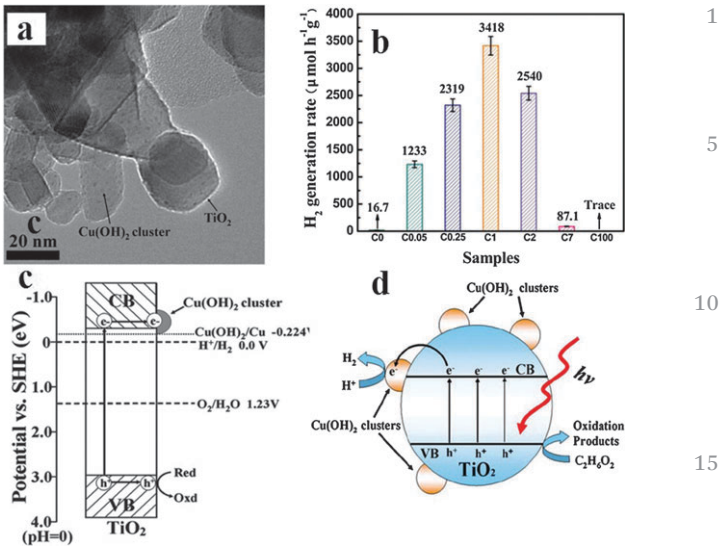

Fig. 3 (a) High-magnification TEM images of the $Cu(OH)_2$–TiO_2 composite. (b) Comparison of the photocatalytic activity of the $Cu(OH)_2$–TiO_2 composite with different contents of $Cu(OH)_2$ for the photocatalytic H_2 production in ethylene glycol aqueous solution under UV-LED irradiation. (c) Proposed mechanism for photocatalytic H_2 production under UV light irradiation. (d) Schematic illustration of the charge transfer and separation in the $Cu(OH)_2$ cluster-modified TiO_2 system under UV-LED irradiation. Reprinted with permission from ref. 77. Copyright 2011, Royal Society of Chemistry.

$$Cu + 2e^- + 2H^+ = Cu + H_2 \quad (2)$$

The work by Yu *et al.*[79] showed that $Ni(OH)_2$-modified CdS nanorods exhibited a visible-light H_2-production rate of 5084 μmol h^{-1} g^{-1} (corresponding to a QE of 28%), exceeding that of pure CdS nanorods and 1 wt% Pt-loaded CdS nanorods by more than 145 times and 1.3 times, respectively. Moreover, the photocatalytic H_2-production rate of $Ni(OH)_2$/graphitic-C_3N_4 (g-C_3N_4) approached that of 1 wt% Pt-loaded graphitic-C_3N.[80] Jang *et al.*[150] employed a hydrothermal method to intercalate $Ni(OH)_2$ in the interlayer of titanate nanotubes. The nickel-intercalated titanate nanotubes (Ni–TNT) showed a great enhancement of H_2-production activity compared to pure titanate nanotubes (TNT) in methanol aqueous solution. Furthermore, the above studies showed that in comparison to metallic Ni and NiO, $Ni(OH)_2$ is a more efficient cocatalyst for photocatalytic H_2 production.[79,80,150] Also, $Co(OH)_2$ was shown to be an efficient cocatalyst on the Fe_2O_3 nanoring for photocatalytic H_2-production.[152]

3.2.2 Transition metal sulfides and carbides. To date, many transition metal sulfides, *i.e.* FeS,[97] CoS,[97,153] NiS,[97,112,153–155] NiS_2,[156] CuS,[113,153,157,158] MoS_2,[100,159–161] MoS_3[162] and WS_2,[163] have been reported as excellent candidates for cost-effective cocatalysts, aiming to substitute for noble metals in photocatalytic H_2 evolution. Highly dispersed and ultrafine NiS NPs were loaded onto the CdS surface *via* an easy hydrothermal method, forming NiS/CdS photocatalyst.[112] The H_2-evolution rate achieved using the optimized NiS (1.2 mol%)/CdS in lactic acid solution under visible light (λ > 420 nm) illumination was

as high as 2.18 mmol h^{-1}, which corresponds to a QE of 51.3% and exceeds the rate on pure CdS by more than 35 times. In contrast, the Pt (1 wt%)/CdS photocatalyst can only produce 0.4 mmol H_2 per hour under identical reaction conditions. This remarkable enhancement in the photocatalytic activity resulted from NiS cocatalyst that played an important role in the NiS/CdS photocatalyst by promoting the electron separation and transport from the CB of CdS to the surface NiS NPs as well as by accelerating the electrochemical adsorption and desorption kinetics for H_2 evolution according to eqn (3) and (4):

$$NiS + e^- + H^+ \rightarrow HNiS \quad (3)$$

$$HNiS + e^- + H^+ \rightarrow NiS + H_2 \quad (4)$$

Furthermore, the influence of hydrothermal temperature or duration of loading NiS on the photocatalytic activity was investigated; it was found that high loading temperature or long treatment time led to the aggregation and larger size of NiS NPs on CdS, causing the reduction of its photocatalytic H_2-production activity. NiS was also loaded on $Cd_xZn_{1-x}S$,[153] g-C_3N_4[154] and TiO_2,[155] to boost the photocatalytic activity. Yuan *et al.*[156] reported that NiS_2 NPs as a noble-metal free cocatalyst could enhance the H_2 production rate of $CdLa_2S_4$ photocatalyst by up to 3 times.

Very recently, Zhang *et al.*[113] prepared a CuS/ZnS porous nanosheet photocatalyst by a facile hydrothermal and cation exchange reaction between preformed $ZnS(en)_{0.5}$ nanosheets and $Cu(NO_3)_2$. During the hydrothermal process, CuS clusters spontaneously grew on the surface of ZnS NPs (Fig. 4a) due to its much smaller solution product, thus forming close interconnection with ZnS, which is believed to facilitate the vectorial transfer of photoinduced electrons from ZnS to CuS and consequently, to improve the charge separation and photocatalytic efficiency. On the other hand, this intimate contact between CuS and ZnS could enable the photoinduced interfacial charge transfer (IFCT) from the VB of ZnS to CuS, making the CuS/ZnS photocatalyst responsive to visible light (see Fig. 4c). Due to the above-mentioned reasons, the prepared CuS/ZnS porous nanosheets presented a high photocatalytic H_2-production rate of 4147 μmol h^{-1} g^{-1} at a CuS loading amount of 2 mol% (see Fig. 4b) and a QE of 20% at 420 nm, even in the absence of any noble-metal cocatalyst. The role of CuS as a cocatalyst to extract photogenerated electrons from $Zn_{0.8}Cd_{0.2}S$ for photocatalytc H_2 evolution was confirmed by the transient photovoltage (TPV) results.[158] Wang *et al.*[153] showed that the rate of H_2 evolution over $Cd_{0.4}Zn_{0.6}S$ loaded with NiS, CoS or CuS is comparable to that of the $Cd_{0.4}Zn_{0.6}S$ loaded with 1 wt% Pt cocatalyst. Interestingly, the dispersion of transition metal sulfides, such as FeS, CoS, NiS, Ru_2S_3, Ag_2S, and PdS, in $CuGa_3S_5$ photocatalyst solution also resulted in enhanced photocatalytic H_2-production activity.[97] In particular, the activity of the NiS–$CuGa_3S_5$ system was six times higher than that of $CuGa_3S_5$ alone and three times higher than that of the Rh–$CuGa_3S_5$ system.

MoS_2 is a well-known electrocatalyst for its excellent H_2 evolution reaction (HER) activity which stems from its exposed and under-coordinated edge sites.[100,164] Recently, MoS_2 has also been reported as an efficient cocatalyst on a variety of semiconductor photocatalysts. Li *et al.*[159] loaded MoS_2 on CdS by a conventional impregnation-sulfidation method. The loading of MoS_2 as a cocatalyst on CdS increased its H_2 evolution rate by up to 36 times. Although Pt presented better H_2-activation performance than MoS_2 in electrochemical systems, MoS_2/CdS still showed a higher rate of H_2 evolution than Pt/CdS, suggesting that the intimate contact (or heterogeneous junction) formed between MoS_2 and CdS is of great importance for enhancing its photocatalytic activity. Very recently, Hou *et al.*[100] found that the layered nanojunction formed between MoS_2 and mesoporous g-C_3N_4 (g-CN) played a key role in improving the photocatalytic activity. They proposed that the similar layered structures of MoS_2 and g-CN would minimize the lattice mismatch and favor the planar growth of MoS_2 slabs on the g-CN surface, thus forming a thin-layered heterogeneous nanojunction (Fig. 5a). Such a nanostructure could not only increase the accessible area around the planar interface of the MoS_2 and g-CN, but also decrease the barrier for electron transport through MoS_2, thus promoting electron migration across the interface. Moreover, the thin layers could also improve the light utilization of g-CN by reducing the light-shielding effect of MoS_2. Furthermore, as shown in Fig. 5b, the band structures of g-CN and MoS_2 allow the vectorial transfer of photoinduced electrons from the CB of g-CN to the CB of MoS_2, where electrons maintain enough chemical potential to reduce H^+ to H_2 molecules. Due to the aforementioned reasons, it is not surprising that the loading of MoS_2 on g-CN tremendously increased the photocatalytic H_2-production activity. In particular, the 0.2 wt% MoS_2/g-CN

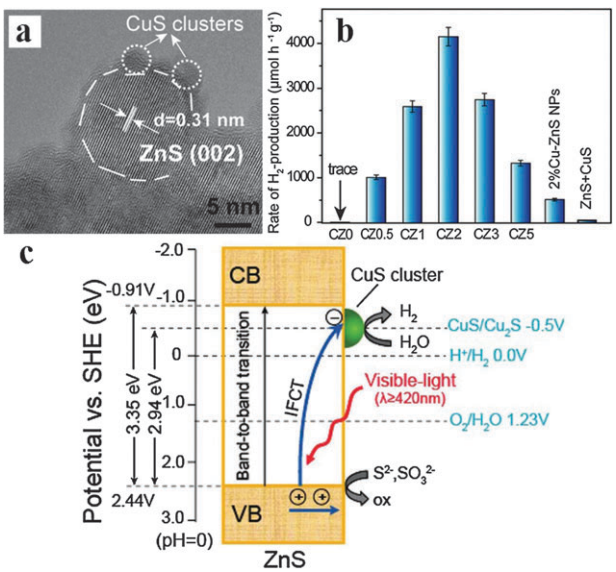

Fig. 4 (a) HRTEM image of CuS/ZnS porous nanosheets. (b) Comparison of the visible-light photocatalytic H_2-production activity of CuS/ZnS porous nanosheets and ZnS samples under visible light (λ > 420 nm) with the mixed aqueous solution containing 0.35 M Na_2S and 0.25 M Na_2SO_3 as sacrificial solution. (c) Schematic illustration of visible-light induced IFCT from the valence band of ZnS to the CuS clusters in the CuS–ZnS system as the proposed mechanism for photocatalytic H_2 production. Reprinted with permission from ref. 113. Copyright 2011, American Chemical Society.

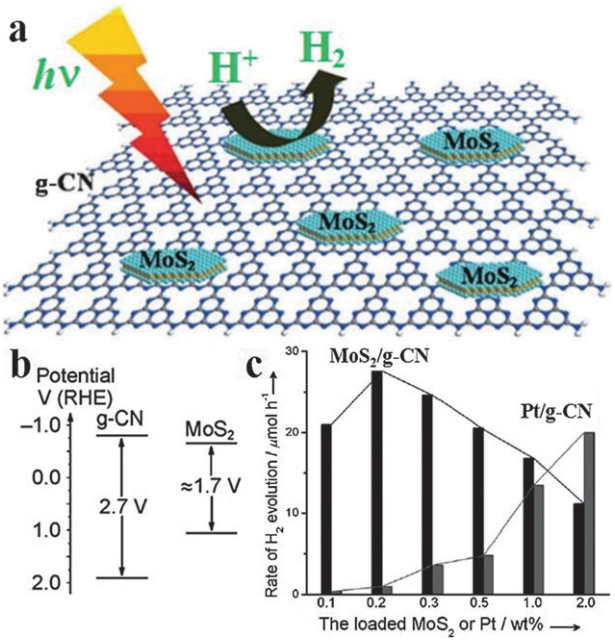

Fig. 5 (a) Schematic illustration of the photocatalytic H_2-evolution process over MoS_2-loaded g-CN under visible-light irradiation. (b) Band energy diagrams for g-CN and thin MoS_2. (c) The rate of H_2 evolution over g-CN loaded with different amounts of MoS_2 or Pt. Reprinted with permission from ref. 100. Copyright 2013, John Wiley & Sons, Inc.

exhibited the highest H_2-production rate with a QE of 2.1% at 420 nm, even much higher than that of 0.5 wt% Pt/g-CN (4.8 μmol h^{-1}, Fig. 5c).

Indeed, the utilization of MoS_2 as a cocatalyst led to remarkable activity improvement of photocatalysts like CdS and g-C_3N_4. However, in the above studies, a conventional impregnation-sulfidation method was applied to load MoS_2 under relatively harsh conditions, such as high temperature, high pressure and use of toxic H_2S as a co-precursor. Hence, a facile, energy-saving and environmental-friendly method is desirable for achieving the successful loading of MoS_2 on semiconductor photocatalysts. Very recently, an *in situ* photo-assisted deposition approach using $(NH_4)_2MoS_4$ as a precursor was developed to decorate MoS_2 on as-prepared $Zn_xCd_{1-x}S$ NPs under mild conditions: room temperature, atmospheric pressure and visible-light irradiation.[160] During the photo-assisted deposition process, the electrons generated in the CB of $Zn_xCd_{1-x}S$ by light irradiation reduced the $[MoS_4]^{2-}$ in the reaction solution to form MoS_2 on the surface of $Zn_xCd_{1-x}S$ *via* the reaction in eqn (5), yielding MoS_2-loaded $Zn_xCd_{1-x}S$ photocatalysts:

$$[MoS_4]^{2-} + 2e^- \rightarrow MoS_2 + 2S^{2-} \quad (5)$$

Surprisingly, the optimized MoS_2-loaded $Zn_{0.2}Cd_{0.8}S$ even showed 210 times faster H_2-generation rate (0.42 mmol H_2 g_{cat}^{-1} h^{-1}) than that obtained with the untreated $Zn_{0.2}Cd_{0.8}S$ photocatalyst. Frame and co-workers[161] reported a new preparation of MoS_2 nanosheets by chemical exfoliation of bulk MoS_2 and the self-assembly of the as-prepared MoS_2 nanosheets with CdSe nanoribbons in the solution phase. The synthesized MoS_2-modified CdSe nanoribbons displayed a great enhancement of photocatalytic activity as compared to pure CdSe.

Tang *et al.*[162] reported the coating of amorphous MoS_3 on the CdSe-seeded CdS nanorods *via* a facile one-step thermal process for photocatalytic H_2 production. The maximum H_2-production activity of 100 mmol h^{-1} g^{-1} of H_2 was obtained, with a QE of 10% under 450 nm light irradiation. This activity is far higher than that found for the crystalline MoS_2 deposited on cadmium chalcogenides.[159–161] Characterization studies revealed that during the induction period, the initial MoS_3 precatalyst was photoreduced to form an under-coordinated species structurally similar to MoS_3, distinct from MoS_2. This reduced MoS_3 was shown for the first time as a highly active cocatalyst for photocatalytic H_2 evolution. Similar to MoS_2, WS_2 is also a transition metal disulfide which has a layered crystal structure and presents good H_2-activation performance. Thus, a great improvement of photocatalytic H_2-production activity was also observed on WS_2-loaded CdS in lactic acid under visible-light irradiation.[163] Furthermore, a novel tungsten carbide (WC) cocatalyst has been developed to replace noble-metal Pt in photocatalytic H_2 evolution.[165] In the study, the as-prepared WC NPs were combined with CdS by a precipitation and hydrothermal method. The resulting WC–CdS composite photocatalyst even showed a comparable H_2-evolution rate to that of Pt-loaded CdS; WC NPs acted as proton-reduction sites and induced rapid electron diffusion from CdS to WC NPs.

Most of the above cocatalysts in this section are based on the oxides, hydroxides and sulfides of first-row transition metals Co, Ni and Cu. Among them, Ni-based cocatalysts, *e.g.* NiO_x, $Ni(OH)_2$ and NiS, are the most active and are proven to be generally effective on different types of semiconductor photocatalysts. Particularly, both $Ni(OH)_2$ and NiS can tremendously raise the photocatalytic activity of TiO_2, CdS and g-C_3N_4, implying their general utility as effective cocatalysts over oxide, sulfide and nitride semiconductors. More strikingly, the above $Ni(OH)_2$ or NiS loaded photocatalysts displayed comparable or even higher H_2-production rates than their Pt-loaded counterparts, suggesting that $Ni(OH)_2$ and NiS are excellent substitutes for Pt. Among the early transition metal Mo- and W-based cocatalysts, MoS_2 has been extensively studied and found to be a powerful cocatalyst for photocatalytic H_2 evolution. For example, both MoS_2/CdS and MoS_2/g-C_3N_4 showed higher H_2-production efficiency than Pt/CdS and Pt/g-C_3N_4, respectively, indicating that MoS_2 is an excellent candidate for Pt replacement. A strong enhancement in the photocatalytic activity achieved in the case of the low-priced and earth-abundant cocatalysts over noble-metal Pt is believed to be mainly associated with the construction of an intimate interface/junction between the semiconductor and the cocatalyst, which greatly expedites the interfacial electron transfer from the semiconductor to the cocatalyst in H_2 evolution. Thus, the design and fabrication of a high-quality junction structure between the semiconductor and the cocatalyst is of great importance for achieving remarkable photocatalytic activity.

3.3 Nanocarbon-based cocatalysts for H_2 evolution

Conventional cocatalysts are transition metals or their compounds loaded as nanoparticles on semiconductor photocatalysts. An important alternative to transition metals are metal-free carbon nanomaterials, which have many unique properties, such as high electrical conductivity, large surface area and novel morphologies. Besides, they are very cheap, abundant, stable and non-toxic. Actually, extensive studies have shown that carbon nanomaterials could be used either as cost-effective cocatalysts or as excellent support and conductive materials in composite cocatalysts to couple with semiconductors for photocatalytic H_2 production.

3.3.1 Carbon nanotubes. Carbon nanotubes (CNTs) exhibit many attractive characteristics, including one-dimensional (1D) structure, large specific surface area, extraordinary mechanical properties and good electronic properties.[166] In particular, multi-walled CNTs are 1D carbon-based ideal nanocylindrical structures, in which electrons can move freely without any scattering from atomic defects.[167] In addition, their long-range conjugated π electrons are beneficial for accelerating the electron transfer.[168] Thus, CNTs could play the role of a metal cocatalyst accepting and transferring photogenerated electrons from the semiconductor photocatalyst to H_2-evolution active sites on their surface.

Yu and coworkers[81] have synthesized a new visible-light photocatalyst, multiwalled CNT-modified $Cd_{0.1}Zn_{0.9}S$ (CNT–$Cd_{0.1}Zn_{0.9}S$), *via* a facile one-pot hydrothermal method. The photocatalytic H_2-production activity of $Cd_{0.1}Zn_{0.9}S$ was tremendously improved by loading the specified amount of CNTs as a cocatalyst. This study showed that 0.25 wt% CNT/$Cd_{0.1}Zn_{0.9}S$ displayed the highest photocatalytic H_2-production rate of 1563.2 μmol h^{-1} g^{-1} with an apparent QE of 7.9% at 420 nm even without any noble metal cocatalyst, exceeding that of pure $Cd_{0.1}Zn_{0.9}S$ by more than 3.3 times. The dominant contribution of CNTs in CNT–$Cd_{0.1}Zn_{0.9}S$ composites to enhance photocatalytic activity is related to their function as electron acceptors and transfer channels, which result in the enhancement of the charge separation efficiency. Moreover, the aforementioned CNT–$Cd_{0.1}Zn_{0.9}S$ exhibited an excellent stability against photo-corrosion under visible-light irradiation. Peng *et al.*[82] reported that a mutiwalled CNT–CdS nanocomposite showed much higher photocatalytic H_2-production efficiency and photostability than pure CdS NPs.

3.3.2 Graphene. Similar to CNTs, graphene, a two-dimensional (2D) network of hexagonally structured sp^2-hybridized carbon atoms,[169] also shows excellent properties, such as fast mobility of charge carriers, exceptional conductivity, large theoretical specific surface area, and good optical transmittance.[170–173] More importantly, graphene behaves like metals due to its large work function (4.42 eV).[174] As a result, graphene could accept photogenerated electrons from CBs of most semiconductors. Meanwhile, the reduction potential of graphene/graphene$^{\bullet-}$ (−0.08 V *vs.* SHE, pH 0) is more negative than that of H^+/H_2 (0.00 V *vs.* SHE, pH 0),[83] which favors the reduction of H^+ to H_2 molecules on graphene sheets. Therefore, graphene could function as an efficient and cost-effective cocatalyst to promote electron separation and transfer from semiconductors and catalyze the proton reduction on its surface.

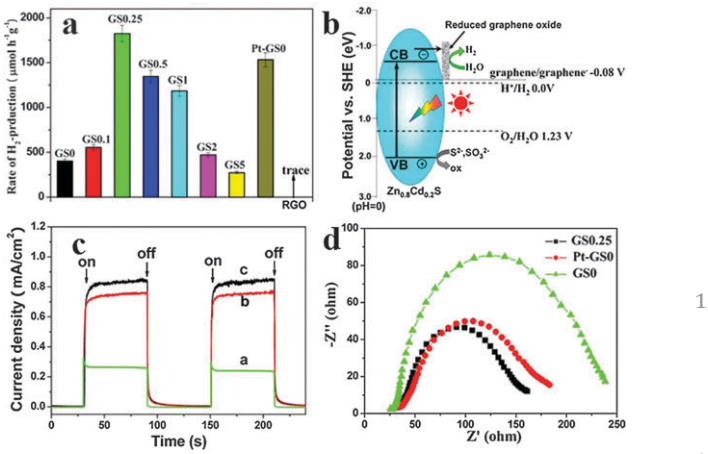

Fig. 6 (a) Comparison of the photocatalytic H_2-production activity under simulated solar irradiation over RGO–$Zn_{0.8}Cd_{0.2}S$ with different contents of RGO, Pt-GS0 (1 wt% Pt loaded $Zn_{0.8}Cd_{0.2}S$), and RGO samples. (b) Proposed mechanism for photocatalytic H_2-production under simulated solar irradiation. (c) Transient photocurrent responses and (d) Nyquist plots for $Zn_{0.8}Cd_{0.2}S$, Pt-GS0 and RGO–$Zn_{0.8}Cd_{0.2}S$ samples. Reprinted with permission from ref. 83. Copyright 2012, American Chemical Society.

Recently, Zhang *et al.*[83] have utilized a facile coprecipitation-hydrothermal reduction method to fabricate the noble metal-free reduced graphene oxide (RGO)–$Zn_xCd_{1-x}S$ nanocomposite. Under simulated one-sun (AM 1.5G) irradiation, this nanocomposite exhibited a remarkable H_2-production rate of 1824 μmol h^{-1} g^{-1} in Na_2S and Na_2SO_3 aqueous solution and a high QE of 23.4% at 420 nm, which is even better than that of 1 wt% Pt-loaded $Zn_{0.8}Cd_{0.2}S$ (Fig. 6a). Such an extraordinary visible-light photocatalytic activity is due to the presence of RGO, which serves as an efficient cocatalyst to collect and transport the photogenerated electrons from the CB of $Zn_{0.8}Cd_{0.2}S$, inhibit electron–hole recombination and supply a large number of active sites on its surface for water reduction (Fig. 6b). The above charge-transfer mechanism is further proved by the transient photocurrent response (TPR) and electrochemical impedance spectra (EIS) data. As shown in Fig. 6c, RGO-$Zn_{0.8}Cd_{0.2}S$ shows the highest transient photocurrent, suggesting that RGO could effectively suppress charge carrier recombination. Moreover, as compared to pure $Zn_{0.8}Cd_{0.2}S$ and Pt-loaded $Zn_{0.8}Cd_{0.2}S$ electrodes, RGO–$Zn_{0.8}Cd_{0.2}S$ features the smallest semicircle in EIS spectra (Fig. 6d), indicating the fastest interfacial electron transfer. Both the TPR and EIS results confirmed that the presence of RGO in the system benefits charge transfer and reduces charge recombination. The above results demonstrate that RGO is a promising cocatalyst for replacing noble metals in photocatalytic H_2 production.

In order to achieve remarkable photocatalytic H_2-production performance, an intimate contact between graphene cocatalyst and semiconductor photocatalyst is very important. For example, Xiang *et al.*[84] have synthesized graphene-modified TiO_2 nanosheets with exposed (001) facets (graphene–TiO_2) as a

noble-metal-free photocatalyst for H_2 production. Under UV light irradiation, the 1 wt% graphene–TiO_2 composite reached the highest H_2-production rate of 736 μmol h^{-1} g^{-1}, exceeding the rate observed on pure TiO_2 by a factor of 41. This enhancement in H_2-production rate was possible because of intimate interactions between TiO_2 nanosheets and graphene; a face-to-face orientation in this composite structure promotes the migration of electrons from TiO_2 to graphene. Similarly, Zhou *et al.*[85] reported the *in situ* controlled growth of $Znln_2S_4$ nanosheets on RGO nanosheets for enhanced visible-light photocatalytic H_2 production. The sheet-on-sheet structure created a notable synergetic effect between the two layers. Fan *et al.*[86] prepared a nanocomposite of P25 TiO_2 and RGO by three different techniques, including UV-assisted photocatalytic reduction, hydrazine reduction, and hydrothermal method. They found that the P25–RGO nanocomposite prepared by the hydrothermal method induced stronger interactions between TiO_2 and RGO, thus giving the highest photocatalytic H_2-production activity. Ye *et al.*[175] compared the photocatalytic activity of CdS–graphene and CdS–carbon nanotubes under the same conditions. They attributed the higher activity of CdS–graphene to the stronger interactions or the larger contact interface between CdS and graphene. Lv and coworkers[176] reported that CdS-sulfonated graphene could afford a higher photocatalytic H_2-generation rate than the CdS–Pt composite; also, the H_2-generation rate of P25–RGO accounts for 45% of that obtained for the P25–Pt composite, which confirms the great potential of inexpensive graphene as a cocatalyst to achieve highly efficient H_2 evolution without noble metals. The work by Peng *et al.*[177] also shows that GO could serve as a low-cost cocatalyst to increase the visible-light photocatalytic activity of CdS. Furthermore, Khan *et al.*[178] have constructed two ternary systems of CdS–Al_2O_3–GO and CdS–ZnO–GO, respectively. CdS–Al_2O_3–GO and CdS–ZnO–GO both presented improved photocatalytic H_2-production performance with high QE of 14% and 30%, respectively.

Interestingly, the activity of graphene as a cocatalyst could be further improved by suitable doping with a heteroatom. For instance, Jia and coworkers[179] have coupled CdS with N-doped graphene obtained by thermal treatment of graphene with NH_3. The prepared N-doped graphene–CdS nanocomposite exhibited a much higher photocatalytic H_2-production rate of 210 μmol h^{-1} than that of graphene–CdS (99 μmol h^{-1}) and pure CdS (40 μmol h^{-1}). The N-doped graphene has higher conductivity than graphene due to the doped N impurities, which alter the electron density of states in graphene. Moreover, N-doped graphene as a protective material could inhibit the photo-corrosion of CdS under visible-light illumination (Table 1).

3.3.3 Nanocarbon-based composite cocatalysts for H_2 evolution. Owing to the excellent properties of 1D CNTs and 2D graphene, these materials can also act as supports for the growth or coupling of other H_2-evolution cocatalysts on them, producing CNT-based or graphene-based composite cocatalysts. The synergetic effects between CNT or graphene and supported cocatalysts could significantly raise the activity of coupled photocatalysts. For example, Chai and coworkers[180] showed that the photocatalytic H_2-evolution activity of TiO_2 could be further enhanced with C_{60}-decorated-carbon nanotube composite as a cocatalyst. These authors found that C_{60} clusters decorated on carbon nanotubes can promote the electron transfer from TiO_2 to CNTs and then to C_{60} because fullerenes are stronger electron acceptors than CNTs, and therefore the C_{60}-decorated CNTs can be more beneficial to the photogenerated carrier separation as compared to CNTs or C_{60} alone. Xiang *et al.*[87] have synthesized a ternary TiO_2/MoS_2/graphene hybrid photocatalyst *via* a two-step hydrothermal procedure (Fig. 7a). In the presence of the layered MoS_2–graphene composite as a cocatalyst, the optimized TiO_2–MoS_2–graphene system reached the highest H_2 production rate of 165.3 μmol h^{-1} under UV irradiation and a QE of 9.7% at 365 nm (Fig. 7b). As illustrated in Fig. 7c, the photogenerated electrons in the CB of TiO_2 can be transferred to MoS_2 nanosheets through the graphene sheets which act as a conductive electron transport ''highway'' and then react with the adsorbed H^+ ions at the edges of MoS_2 to form H_2. The notable synergetic effect between MoS_2 nanosheets and graphene led to many advantages of MoS_2/graphene cocatalyst, including suppression of charge recombination, improvement of interfacial charge transfer, and an increase in the number of active adsorption sites and photocatalytic reaction centers. The work by Min *et al.*[181] further demonstrated that MoS_2/RGO could serve as a highly efficient cocatalyst for H_2 evolution in an Eosin Y-sensitized photocatalytic system under visible-light irradiation. It was found that the two dimensional RGO sheets not only provide a confined substrate for the selective growth of limited-layer MoS_2 cocatalyst with a large number of exposed catalytic sites but also form the interconnected two-dimensional conductive networks for efficiently transferring photogenerated electrons from the excited dye to the catalytic active sites of MoS_2, thus suppressing the recombination processes and enhancing the photocatalytic efficiency of hydrogen evolution. Lv *et al.*[182] have investigated the synergetic effect of Cu and graphene as a cocatalyst on TiO_2 for photocatalytic H_2 evolution in the presence of methanol as a sacrificial reagent. The hydrogen evolution efficiency of the Cu–graphene synergetic cocatalyst was about 5 times higher than that of a pure graphene cocatalyst, and was comparable to that of the systems containing the well-known Pt cocatalyst. All the above encouraging results show the huge potential of nanocarbon-based materials as a novel type of cocatalysts for photocatalytic H_2 production.

3.4 Hydrogenase and artificial molecular cocatalysts for H_2 evolution

3.4.1 Hydrogenases. Hydrogenases are natural enzymes capable of efficiently catalyzing the reversible reduction of protons to molecular hydrogen with remarkable activity in many micro-organisms. As H_2-activation catalysts, hydrogenase enzymes exhibit unique properties, including low activation energies and a wide range of O_2 sensitivities, while using organometallic catalytic sites composed of earth-abundant elements (Fe, Ni, S, C, N, and O).[88] Therefore, hydrogenases are attractive catalysts which could be incorporated into photoactive materials and devices for hydrogen evolution.

Table 1 Inorganic earth-abundant cocatalysts for photocatalytic H_2-evolution half reactions

Photocatalyst	Cocatalyst	Loading method	Light source[a]	Reactant solution[b]	H_2 evolution: Activity (μmol h^{-1} g^{-1})	H_2 evolution: Quantum efficiency (%)	H_2 evolution: Stability	Enhancement factor[c]	Ref. (year)
TiO_2	Co	Chemical reduction	UV-Vis (H)	TEOA	1160		>18 h		124 (2012)
	Ni	Chemical reduction			~1160		>6 h		
	Pt	Chemical reduction			3667				
TiO_2	Ni	Photoreduction	UV-Vis (Xe)	Methanol	2547	8.1 (365 nm)		135	108 (2013)
$La_{0.02}Na_{0.98}TaO_3$	Ni	Impregnation	$\lambda \geq 250$ nm (Hg)	Methanol	29 200			10.1	117 (2011)
	NiO_x	Impregnation			26 940		>40 h	9.3	
CdS–titanate	Ni	Photoreduction	$\lambda \geq 420$ nm (Xe)	Ethanol	11 038	21 (420 nm)	>15 h	77	125 (2013)
CNT–TiO_2	Ni	Sol–gel	780 > λ > 380 nm (MH)	Methanol	38.1		>4 h		137 (2006)
Nb_2O_5	Cu	Impregnation	UV-Vis (H)	Methanol	1572			4.8	64 (2011)
	NiO	Impregnation			709			2.2	
	Pt	Photoreduction			4647			14.2	
	Au	Photoreduction			2091			6.4	
TiO_2	Cu	Impregnation	UV-Vis (Xe)	Methanol	12 779			6.6	140 (2013)
TiO_2	NiO	Sol–gel	UV-Vis (Hg)	Methanol	813		<5 h	1.9	110 (2005)
$La_2Ti_2O_7$	NiO_x	Impregnation	UV-Vis (Hg)	TMAH	5328				131 (2002)
$KNbO_3$/CdS	NiO_x	Impregnation	λ > 400 nm (Hg–Xe)	IPA	150	4.4 (λ > 400 nm)	>40 h	3	143 (2008)
$KNbO_3$/CdS	NiO_x	Impregnation	λ > 400 nm (Hg–Xe)	IPA	203.5	8.8 (λ > 400 nm)	>40 h	10.2	144 (2007)
	Pt	Photoreduction			147			7.4	
TiO_2	CuO	Impregnation	365 nm (LED)	Glycerol	2061	13.4 (365 nm)	>8 h	129	111 (2011)
TiO_2	CuO	Adsorption-calcination	UV-Vis (Hg)	Methanol	71 600		>5 h		114 (2011)
	CuO	Impregnation			64 200		>5 h		
TiO_2	CuO	Impregnation	Natural solar irradiation	Glycerol	99 823		>4 h	21.6	115 (2013)
TiO_2	CuO	Sol–gel	UV-Vis (Hg)	Methanol	1800				145 (2005)
	PdO	Sol–gel			2100				
	Au	Sol–gel			2785				
TiO_2	CuO	Impregnation	UV-Vis (Hg)	Methanol	18 500		<10 h		147 (2009)
TiO_2	Cu_2O	Chemical reduction	UV-Vis (Hg)	Methanol	20 000		<5 h	222	148 (2010)
	CuO	Impregnation			9000		<5 h	100	
	CuO	Sol–gel					<5 h		
	Cu	Photoreduction					<5 h		
TiO_2	$Cu(OH)_2$	Precipitation	365 nm (LED)	Ethylene glycol	3418	13.9 (365 nm)	>6 h	205	77 (2011)
TiO_2	$Cu(OH)_2$	Hydrothermal-precipitation	UV-Vis (Hg)	Methanol	14 940		>10 h		116 (2013)
TiO_2	$Ni(OH)_2$	Precipitation	365 nm (LED)	Methanol	3056	12.4 (365 nm)		223	78 (2011)
CdS	$Ni(OH)_2$	Precipitation	$\lambda \geq 420$ nm (Xe)	TEOA	5084	28 (420 nm)	>6 h	145	79 (2011)
	Pt	Photoreduction			3896			111	
g-C_3N_4	$Ni(OH)_2$	Precipitation	$\lambda \geq 400$ nm (Xe)	TEOA	152	1.1 (420 nm)	<12 h		80 (2013)
	Pt	Photoreduction			164				
α-Fe_2O_3	$Co(OH)_2$	Chemical-precipitation	UV-Vis (Hg–Xe)	Ethanol	546		>2.5 h	1.6	152 (2013)
$CuGa_3S_5$	NiS	*In situ* precipitation	$\lambda \geq 420$ nm (Xe)	Na_2S, Na_2SO_3	980			3.3	97 (2010)
	FeS	*In situ* precipitation			760			2.5	
	CoS	*In situ* precipitation			460			1.5	
	CuS	*In situ* precipitation			260			0.9	
	Ru_2S_3	*In situ* precipitation			580			1.9	
	Ag_2S	*In situ* precipitation			520			1.7	
	PdS	*In situ* precipitation			420			1.4	
	Rh	*In situ* precipitation			800			2.7	
$Cd_{0.4}Zn_{0.6}S$	NiS	*In situ* precipitation	$\lambda \geq 420$ nm (Xe)	Na_2S, Na_2SO_3	1200			5	153 (2012)
	CoS	*In situ* precipitation			1100			4.6	
	CuS	*In situ* precipitation			1000			4.2	
	Pt	Photoreduction			1210			~5	
CdS	NiS	Hydrothermal	$\lambda \geq 420$ nm (Xe)	Lactic acid	7267	51.3 (420 nm)	<12 h	34.6	112 (2010)
g-C_3N_4	NiS	Hydrothermal	$\lambda \geq 420$ nm (Xe)	TEOA	482	1.9 (440 nm)	>4 h	250	154 (2013)
TiO_2	NiS	Solvothermal	UV-Vis (Xe)	Lactic acid	698		>5 h	30	155 (2012)
$CdLa_2S_4$	NiS_2	Hydrothermal	$\lambda \geq 420$ nm (Xe)	Na_2S, Na_2SO_3	2500	1.6 (420 nm)	<40 h	3.1	156 (2013)
	Pt	Photoreduction			1300			1.6	
ZnS	CuS	Hydrothermal	$\lambda \geq 420$ nm (Xe)	Na_2S, Na_2SO_3	4147	20 (420 nm)	<12 h		113 (2011)

Table 1 (*continued*)

Photocatalyst	Cocatalyst	Loading method	Light source[a]	Reactant solution[b]	H_2 evolution: Activity (μmol h^{-1} g^{-1})	Quantum efficiency (%)	Stability	Enhancement factor[c]	Ref. (year)
$Zn_{0.5}Cd_{0.5}S$	CuS	Microwave-hydrothermal	$\lambda \geq 420$ nm (Xe)	Na_2S, Na_2SO_3	4638.5	20.9 (420 nm)	<12 h	7	157 (2013)
$Zn_{0.8}Cd_{0.2}S$	CuS	Hydrothermal	UV-Vis (Xe)	Na_2S, Na_2SO_3	2792	36.7 (420 nm)		4.4	158 (2013)
g-C_3N_4	MoS_2	Impregnation-sulfidation	$\lambda \geq 420$ nm (Xe)	Lactic acid	1030	2.1 (420 nm)	<16 h		100 (2013)
	Pt	Photoreduction			240				
CdS	MoS_2	Impregnation-sulfidation	$\lambda \geq 420$ nm (Xe)	Lactic acid	5400			36	159 (2008)
$Zn_{0.2}Cd_{0.8}S$	MoS_2	*In situ* photo-assisted deposition	$\lambda \geq 420$ nm (Xe)	Na_2S, Na_2SO_3	420		>18 h	210	160 (2013)
CdSe	MoS_2	Dispersion–adsorption	$\lambda \geq 400$ nm (Xe)	Na_2S, Na_2SO_3	890		>5 h	3.7	161 (2010)
CdSe/CdS	MoS_3	Thermal deposition	450 nm (Hg–Xe)	TEOA	100 000	10 (450 nm)			162 (2011)
CdS	WS_2	Impregnation-sulfidation	$\lambda \geq 420$ nm (Xe)	Lactic acid	4200	5 (420 nm)	<15 h	28	163 (2011)
	Pt	Photoreduction			3550			23.7	
$Cd_{0.1}Zn_{0.9}S$	CNT	Hydrothermal	$\lambda \geq 420$ nm (Xe)	Na_2S, Na_2SO_3	1564	7.9 (420 nm)	>15 h	3.3	81 (2012)
CdS	CNT	Hydrothermal	$\lambda \geq 420$ nm (Xe)	Na_2S, Na_2SO_3	4977	2.16 (420 nm)	>15 h	1.8	82 (2011)
$Zn_{0.8}Cd_{0.2}S$	RGO	Coprecipitation-hydrothermal	AM 1.5G (Xe)	Na_2S, Na_2SO_3	1824	23.4 (420 nm)	>12 h	4.5	83 (2012)
	Pt	Photoreduction			1531			3.8	
TiO_2	RGO	Microwave-hydrothermal	UV-Vis (Xe)	Methanol	736	3.1 (365 nm)		41	84 (2011)
$ZnIn_2S_4$	RGO	Solvothermal	$\lambda \geq 420$ nm (Xe)	Na_2S, Na_2SO_3	1632		<12 h	3.7	85 (2013)
TiO_2	RGO	Hydrothermal	UV-Vis (Xe)	Methanol	740		<16 h	11	86 (2011)
CdS	RGO	Hydrothermal	$\lambda \geq 420$ nm (Xe)	Na_2S, Na_2SO_3	700	4.8 (420 nm)	>15 h	4.8	175 (2012)
	CNT	Hydrothermal			520		>3 h	3.6	
CdS	GO	Precipitation	$\lambda \geq 420$ nm (Xe)	Na_2S, Na_2SO_3	3140		>15 h	1.3	177 (2012)
CdS/Al_2O_3	GO	Solid-state ground	Visible (TH)	Na_2S, Na_2SO_3	1750	14			178 (2012)
CdS/ZnO	GO	Solid-state ground	Visible (TH)	Na_2S, Na_2SO_3	3755	30			178 (2012)
CdS	N doped-RGO	Precipitation-calcination	$\lambda \geq 420$ nm (Xe)	Na_2S, Na_2SO_3	1050		>30 h	5.3	179 (2011)
TiO_2	C_{60}–CNT	Hydrothermal	UV-Vis (Xe)	TEOA	6510		>15 h	3.1	180 (2013)
TiO_2	MoS_2–RGO	Hydrothermal	UV-Vis (Xe)	Ethanol	2066	9.7 (365 nm)	>12 h		87 (2012)
TiO_2	Graphene–Cu	Hydrothermal and *in situ* photo-assisted deposition	UV-Vis (Hg)	Methanol	63 750		<60 h		182 (2012)

[a] H: halogen lamp, Xe: xenon lamp, Hg: mercury lamp, MH: metal halide light, Hg–Xe: mercury xenon arc lamp, TH: tungsten halogen lamp. [b] TEOA: triethanolamine, TMAH: tetramethylammonium hydroxide, IPA: isopropanol. [c] Enhancement factor is calculated from the activity enhancement of photocatalysts loaded with the optimal amount of cocatalysts over photocatalysts without the loading of cocatalysts.

Very recently, it has been reported that hydrogenases could be employed as cocatalysts to combine with semiconductors for photocatalytic H_2 production.[88,89]

Brown *et al.*[88] have investigated the self-assembly, charge-transfer kinetics, and photocatalytic performance of a hybrid complex composed of Clostridium acetobutylicum [FeFe]-hydrogenase I (CaI) and CdTe nanocrystals capped with 3-mercaptopropionic acid (MPA). As demonstrated in Fig. 8, the molecular assembly of CdTe and CaI was mediated by electrostatic interactions and resulted in stable as well as enzymatically active complexes for photocatalytic H_2 evolution under visible-light illumination. Photoluminescence (PL) spectroscopy results confirmed the rapid intramolecular photoexcited electron transfer in the complex from CdTe to CaI, which acts as a cocatalyst for reducing protons to H_2. They also found that the relative contribution of electron transfer to CdTe relaxation was strongly affected by the CdTe/CaI molar ratio, with a lower CaI surface coverage resulting in a larger contribution of electron transfer and higher H_2 production rate. The optimized CdTe–CaI complex achieved a QE of 9% at 523 nm and 1.8% under AM 1.5 white light irradiation using ascorbic acid as a hole scavenger. The observed turnover frequency (TOF) of H_2 production under

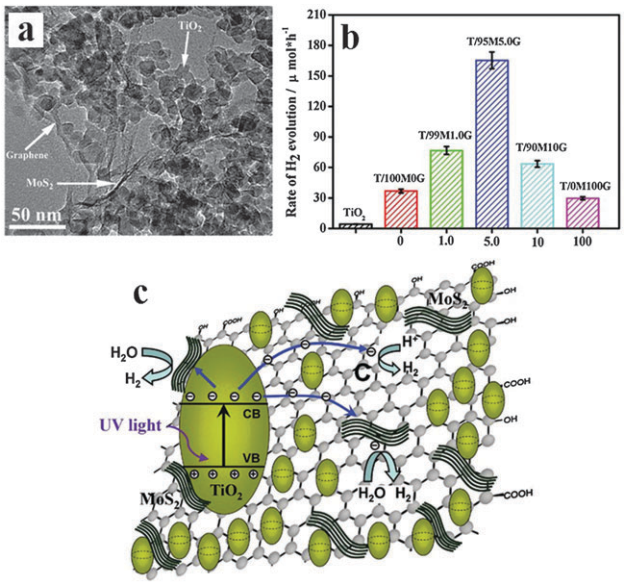

Fig. 7 (a) TEM image of TiO_2 nanocrystals grown on layered MoS_2–graphene (MG) hybrids (T/95M0.5G). (b) Comparison of the photocatalytic H_2-production activity under UV irradiation over the TiO_2–MG composite photocatalyst with different MoS_2 and graphene contents in the MG hybrid as a cocatalyst. (c) Schematic diagram of charge carrier separation and photocatalytic H_2 production on the ternary TiO_2–MG composites under UV-light irradiation. Reprinted with permission from ref. 87. Copyright 2012, American Chemical Society.

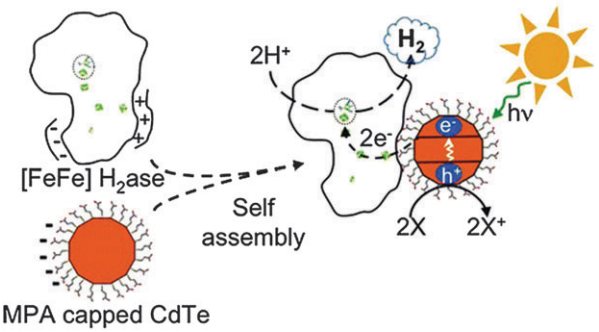

Fig. 8 Schematic illustration of the self-assembly of Clostridium acetobutylicum [FeFe]-hydrogenase I and MPA capped CdTe nanocrystals, and light-induced H_2 production under visible-light illumination of the self-assembled complex. Reprinted with permission from ref. 88. Copyright 2010, American Chemical Society.

white light irradiation was 25 mol H_2 (mol CaI)$^{-1}$ s^{-1}. Based on this work, Brown and coworkers[89] further employed CaI as a H_2-evolution cocatalyst combined with MPA-capped CdS nanorods for photocatalytic H_2 production. Remarkably, the CdS nanorod–CaI complex presented a TOF of 380–900 mol H_2 (mol Hydrogenase)$^{-1}$ s^{-1} and a QE of up to 20% under irradiation at 405 nm. In addition, the total turnover number (TON) of 10^6 was obtained over the CdS nanorod–CaI complex after H_2 evolution for 4 h until inactivation of the complex. This loss of activity is related to the deactivation of CaI, resulting from the oxidative loss of the MPA ligand from the CdS surface by photoexcited holes.

The above studies not only demonstrate the feasibility of coupling biological hydrogenase cocatalysts with inorganic semiconductor photocatalysts for highly efficient H_2 production, but also provide an insight into the rational design and preparation of the hybrid hydrogenase–inorganic semiconductor photocatalyst in the future.

3.4.2 Hydrogenase mimics. Inspired by the extremely high activity of hydrogenases, many research groups are engaged in developing small organometallic molecular catalysts that mimic the catalytic center of hydrogenases. These artificial catalysts are named H_2ase mimics. In the past two decades, several H_2ase mimics, which are coordination compounds of Fe, Co or Ni, have been developed.[183] Among them, dinuclear [FeFe]-H_2ase mimics and cobaloximes have been found to be highly active cocatalysts when integrated with semiconductors for photocatalytic H_2 evolution.[90–92,98,184,185]

For example, Li *et al.*[98] investigated the utilization of a [FeFe]-H_2ase mimic, $[(\mu\text{-SPh-4-NH}_2)_2Fe_2(CO)_6]$ **1** (Fig. 9), as a cocatalyst, ZnS as a photo-harvester and ascorbic acid as an electron donor for photocatalytic H_2 evolution. Surprisingly, this system showed a high visible-light photocatalytic H_2-evolution activity (initial TOF of 100 h^{-1} based on **1**) as well as good stability (a total TON of more than 2607 for up to 38 h). Furthermore, it is noteworthy that the combination of CdS with **1** does not possess photocatalytic H_2-evolution activity, since the CB potential of CdS (−0.9 *vs.* NHE, pH 7) is not sufficiently negative for the first redox potential of **1** (−1.05 V *vs.* NHE, pH 7), indicating that the energy band matching is essential for the efficient electron transfer from semiconductors to molecular cocatalysts for H_2 production. Although [FeFe]-H_2ase mimics possess good H_2-evolution activity, for most of them photocatalytic H_2 production must be carried out in organic solvents or in a mixture of organic solvent and water due to their dissolubility in water, which is neither economic nor environmentally benign. In general, several approaches have been put forward to solve this problem. In one of them, a water-soluble substituent is directly connected to the Fe_2S_2 active site of the [FeFe]-H_2ase mimic. For example, Wang *et al.*[91] have developed an artificial water-soluble [FeFe]-H_2ase mimic **2** by incorporating a cyanide (CN) group to anchor three hydrophilic ether chains to the active site of the [FeFe]-H_2ase mimic for

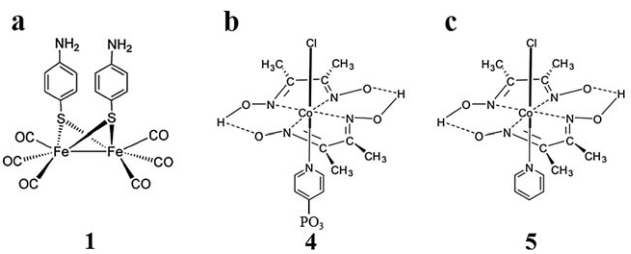

Fig. 9 Structures of artificial molecular cocatalysts: (a) $[(\mu\text{-SPh-4-NH}_2)_2Fe_2(CO)_6]$ **1**. (b) $Co^{III}(dmgH)_2(4\text{-}(PO_3)py)Cl$ **4**. (c) $Co^{III}(dmgH)_2pyCl$ **5**. (a) Reprinted with permission from ref. 98. Copyright 2012, John Wiley & Sons, Inc. (b) Reprinted with permission from ref. 90. Copyright 2012, American Chemical Society. (c) Reprinted with permission from ref. 184. Copyright 2011, Elsevier.

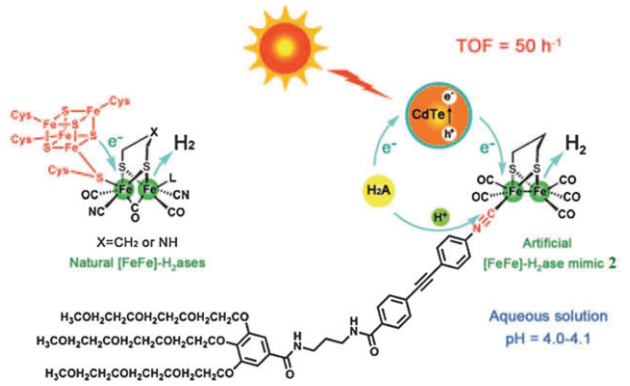

Fig. 10 The structure of natural [FeFe]-H_2ase, artificial [FeFe]-H_2ase mimic **2** and schematic illustration of H_2 photogeneration over **2** coupled with CdTe QDs. Reprinted with permission from ref. 91. Copyright 2011, John Wiley & Sons, Inc.

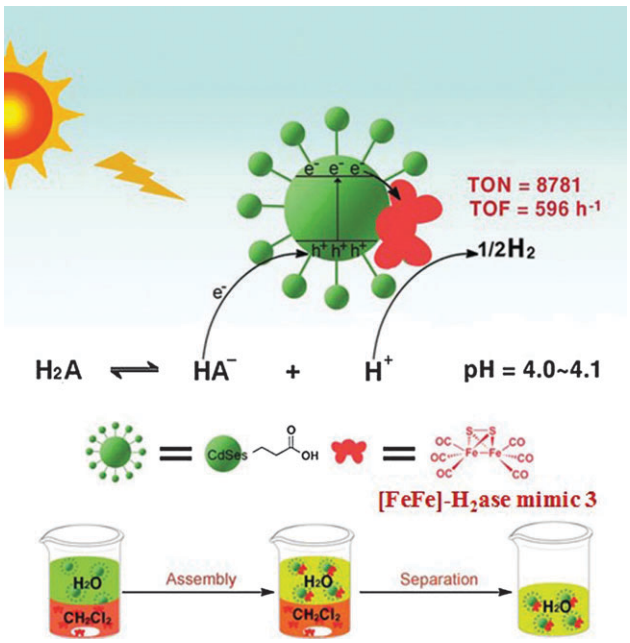

Fig. 11 The interface-directed assembly of CdSe/[FeFe]-H_2ase and its H_2 photogeneration. Reprinted with permission from ref. 92. Copyright 2013, Royal Society of Chemistry.

improving its solubility in water (see Fig. 10). The developed [FeFe]-H_2ase mimic **2** was coupled with CdTe QDs for photocatalytic H_2 production in aqueous solution containing ascorbic acid as an electron donor. This system was able to achieve the production of 786 mmol (17.6 mL) H_2 after 10 hours of irradiation ($\lambda > 400$ nm) in purely aqueous solution, with TON and TOF values of up to 505 and 50 h^{-1} based on **2**, respectively. In another case, Wu *et al.*[92] utilized a novel strategy for interface-directed assembly of [FeFe]-H_2ase mimic **3** onto CdSe QDs as a water-soluble artificial photosynthetic system (Fig. 11). The resulting photocatalytic system showed a very high efficiency for H_2 evolution with a TON of 8781 and an initial TOF of 596 h^{-1} *vs.* **3** under visible-light illumination in water. The present work demonstrated that the intimate contact and strong interactions are particularly important for enhancing the performance of photocatalytic H_2 evolution with the help of artificial [FeFe]-H_2ase systems.

Cobaloximes are another efficient family of H_2-evolution catalysts, which contain a coordinated Co^{III} ion as the redox platform and an –OH group in the second coordination sphere as the proton relay position. Recently, cobaloximes have been examined as effective cocatalysts in heterogeneous photocatalytic H_2 evolution. For instance, Huang *et al.*[90] have anchored **4** (Fig. 9) as a cocatalyst on the surface of CdSe–ZnS core–shell quantum dots (QDs) *via* a phosphonate linkage, producing a CdSe–ZnS QD–cobaloxime hybrid system. Strikingly, visible-light illumination ($\lambda > 400$ nm) of this hybrid system gave a TON of more than 10 000 H_2 per QD in 10 h, in the presence of triethylamine hydrochloride as a proton source and triethanolamine as a sacrificial electron donor. The efficient electron transfer from light-excited QDs to surface-bound cobaloxime cocatalyst proceeds much faster than charge recombination in QDs, which was revealed by optical transient absorption spectroscopy. Subsequently, electrons harvested by cobaloxime led to its reduction from Co^{III} ground state to Co^{II} and Co^{I} species, which further reduced protons to H_2 molecules. Li and coworkers[184] have successfully constructed a hybrid photocatalytic system using CdS as a photosensitizer, **5** (Fig. 9) as a H_2-evolution cocatalyst, and triethanolamine as a sacrificial electron donor. This system exhibited a TON of up to 171 based on **5** and a QE of 9.1% at 420 nm, indicating its excellent photocatalytic H_2-evolution activity. Cao *et al.*[185] reported an economic and noble-metal-free artificial photosynthetic system, consisting of g-C_3N_4 as a photocatalyst and **5** as a cocatalyst for H_2 generation.

3.4.3 *In situ* formed Ni-based molecules. Very recently, several water-soluble Ni-based complexes have been developed as highly durable and active molecular cocatalysts for photocatalytic H_2 evolution.[93,94,186] These complexes could be easily synthesized *via* an *in situ* coordination reaction between metal ions and small water-soluble organic molecules in purely aqueous solution. Thus, no toxic organic solvent is needed to help dissolve these complexes in photocatalytic systems, which is both environmental-friendly and cost-effective.

Dong *et al.*[186] have reported *in situ* synthesis of a robust and efficient Ni-based molecular cocatalyst by the addition of $NiCl_2$ into an aqueous solution containing triethanolamine (TEOA), forming a stable complex of $[Ni(TEOA)_2]Cl_2$. The system consisting of $[Ni(TEOA)_2]Cl_2$ as a cocatalyst, g-C_3N_4 as a light absorber and TEOA as an electron donor displayed a long-term visible-light photocatalytic H_2-production activity for more than 60 h, giving a total amount of 191 μmol H_2 (TON = 281, based on $[Ni(TEOA)_2]Cl_2$). The QE of H_2 production was 1.51% at 400 nm for the $[Ni(TEOA)_2]Cl_2$–g-C_3N_4 system in 10 vol% TEOA aqueous solution. Note that the QE of Pt–g-C_3N_4 under identical conditions is about 1.83% at 400 nm. It was shown that the addition of $[Ni(TEOA)_2]Cl_2$ remarkably decreased the fluorescence intensity of g-C_3N_4, suggesting the electron transfer from the CB of g-C_3N_4 to the Ni complex. Besides, electrochemical

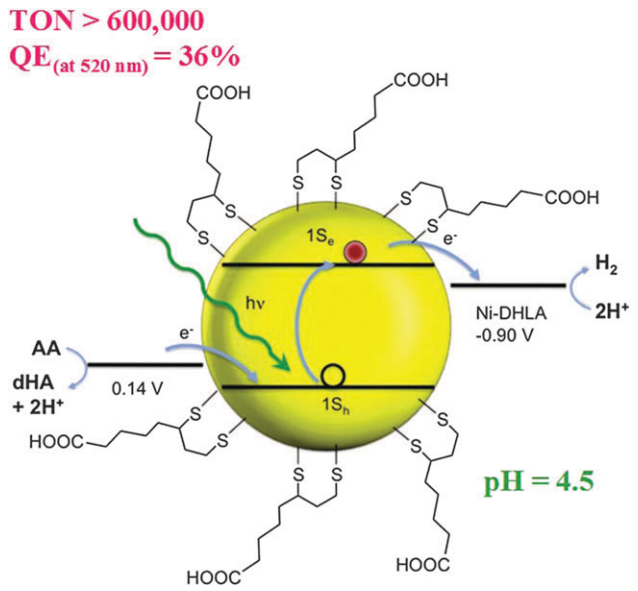

Fig. 12 Cartoon representation of the relevant energies for H_2 production. AA and dHA indicate ascorbic acid and dehydroascorbic acid, respectively. Potentials are shown *versus* that of an NHE at pH 4.5. Reprinted with permission from ref. 93. Copyright 2012, The American Association for the Advancement of Science.

analysis confirmed the high catalytic activity of $[Ni(TEOA)_2]Cl_2$ for water reduction to H_2. Thus, the excellent photocatalytic H_2-production performance of the $[Ni(TEOA)_2]Cl_2$–g-C_3N_4 system is mainly due to the efficient electron transfer from g-C_3N_4 to the Ni complex, which possesses high catalytic activity for reducing water to H_2.

Very recently, a highly active and robust system for solar H_2 generation in water was reported by Han and coworkers.[93] As shown in Fig. 12, this system used a novel water-soluble Ni thiolate complex, Ni^{2+}-dihydrolipoic acid (DHLA), as a cocatalyst, CdSe nanocrystals capped with DHLA as a light absorber and ascorbic acid as an electron donor. Remarkably, this noble-metal-free system presented undiminished activity for at least 360 hours under irradiation at 520 nm, giving a total TON of more than 600 000 (with respect to the Ni complex). Besides, a high QE of over 36% was obtained for this system. In contrast, CdSe nanocrystals without Ni^{2+}-DHLA exhibited much smaller H_2 production under the same conditions because photo-excited electrons from the CB of CdSe could migrate to Ni^{2+}-DHLA, which then catalyzes the hydrogen evolution reaction.

Moreover, Li *et al.*[94] have synthesized a new type of "artificial photocatalyst", a hybrid Ni_h–CdSe–CdS core–shell QD, made from MPA–CdSe QD and $NiCl_2{\cdot}6H_2O$ *in situ* under visible-light illumination at room temperature. Upon visible light illumination, the photogenerated holes (h^+) are capable of oxidizing MPA to sulfide ions (S^{2-}), resulting in the assembly of a CdS shell on the CdSe core *in situ*. Furthermore, the hanging bonds (S^{2-}) distributed on the surface of the QDs coordinate with Ni^{2+} ions intimately to form a Ni complex as a cocatalyst for H_2 generation. Excess of Ni^{2+} ions in the solution would be helpful to avoid the dissociation of Ni^{2+} from the catalyst and to increase its working lifetime, which can be considered as a self-healing process of artificial photocatalysts. Irradiation of the artificial photocatalyst in 2-propanol aqueous solution resulted in efficient H_2 evolution at a constant rate of $\sim$153 μmol h^{-1} mg^{-1}, and an internal QE of 11.2% at 410 nm. The photocatalytic system is stable under visible-light irradiation with TON of 15 340 and 18 000 with respect to the CdSe QDs and nickel, respectively, for 10 h illumination ($\lambda > 400$ nm).

In this section, biological hydrogenases and their artificial mimics as well as the newly developed nickel complexes are introduced as a class of novel H_2-evolution cocatalysts in comparison to the aforementioned inorganic cocatalysts. As shown in Table 2, the employment of hydrogenase CaI as a cocatalyst leads to the highest TOF and QE compared with cocatalysts of artificial molecules due to its intrinsically high activity as a natural biological enzyme. However, this kind of hydrogenase cocatalyst suffers from two inherent drawbacks: (i) scale limitations imposed by using an enzyme from a biological

Table 2 Hydrogenase and artificial molecular cocatalysts for photocatalytic H_2-evolution half reactions

					H_2 evolution				
Photocatalyst	Cocatalyst[a]	Light source[b]	Solvent[c]	Sacrificial reagent[d]	Turnover frequency or activity[e]	Quantum efficiency (%)	Turnover number[f]	Stability	Ref. (year)
CdTe	CaI	AM 3.0 (TH)	Water	AA	25 s^{-1}	9 (532 nm)		<45 min	88 (2010)
CdS	CaI	405 nm (LED) AM 1.5 (LED)	Water	AA	380 s^{-1} 983 s^{-1}	20 (405 nm)	$\sim 10^6$	<6 h	89 (2012)
CdTe	**2**	$\lambda \geq 420$ nm (Hg)	Water	AA	50 h^{-1}		505	<10 h	91 (2011)
CdSe	**3**	$\lambda \geq 400$ nm (Hg)	Water	AA	596 h^{-1}		8781	<80 h	92 (2013)
ZnS	**1**	UV-Vis (Xe)	Water and DMF	AA	100 h^{-1}	2.5 (325 nm)	2607	<38 h	98 (2012)
CdS	**5**	$\lambda > 420$ nm (Xe)	Water and acetonitrile	TEOA		9.1 (420 nm)	171	<15 h	184 (2011)
CdSe	Ni^{2+}-DHLA	520 nm (LED)	Water	AA	7000 h^{-1}	36 (520 nm)	>600 000	>360 h	93 (2012)
CdSe/CdS	Ni complex	$\lambda > 400$ nm (Hg)	Water	IPA	153 mmol h^{-1} g^{-1}	11.2 (410 nm)	18 000	<20 h	94 (2013)
g-C_3N_4	$[Ni(TEOA)_2]Cl_2$	$\lambda > 400$ nm (Xe)	Water	TEOA	6.7 h^{-1}		281	<60 h	186 (2012)

[a] CaI: clostridium acetobutylicum [FeFe]-hydrogenase I, **1**: [FeFe]-H_2ase mimic $[(\mu\text{-SPh-4-NH}_2)_2Fe_2(CO)_6]$, **2**: [FeFe]-$H_2$ase mimic anchored with three hydrophilic ether chains, **3**: [FeFe]-H_2ase mimic $[(\mu\text{-S})_2Fe_2(CO)_6]$, **5**: cobaloxime $Co^{III}(dmgH)_2pyCl$, Ni^{2+}-DHLA: Ni^{2+}-dihydrolipoic acid complex, $[Ni(TEOA)_2]Cl_2$: Ni(II) coordinated with triethanolamine (TEOA) and chloride ion (Cl^-). [b] TH: tungsten halogen lamp, Hg: mercury lamp, Xe: xenon lamp. [c] DMF: dimethyl formamide. [d] AA: ascorbic acid, TEOA: triethanolamine, IPA: isopropanol. [e] Turnover frequency is based on cocatalyst. [f] Turnover number is based on cocatalyst.

organism, and (ii) large geometric size of a hydrogenase that may not allow for high loading of these biocatalysts onto the nanosized photocatalyst to gain sufficient efficiency for industrial application. In contrast, hydrogenase mimics with a much smaller size could be manufactured on a large scale. And they also exhibit good activity though inferior to their biological counterpart at present. However, one key problem with hydrogenase mimics is their dissolubility in water, with the need for toxic organic solvents to help dissolve them. The recent exploration of several Ni complexes synthesized *via* an *in situ* coordination reaction has attracted much attention. These water-soluble Ni complexes are highly efficient and stable. However, for some of them, their molecular structures are yet to be clearly identified, and the relationship between their molecular structures and the performance should be systematically investigated for their rational design and fabrication in the future.

4. Earth-abundant cocatalysts for photocatalytic O_2-evolution half reactions

In comparison to the H_2-evolution half reaction, the O_2-evolution half reaction in overall photocatalytic water splitting is a more challenging step because it involves a four-electron transfer process coupled to the removal of four protons from water molecules to form an oxygen–oxygen bond. As a result, semiconductor photocatalysts usually suffer from low activity for O_2 evolution due to the uphill multi-proton coupled electron transfer and rapid charge recombination.[101,187,188] Consequently, an active cocatalyst is necessary to achieve reasonable efficiency. So far, the most active O_2-evolution cocatalysts are noble-metal oxides (RuO_2 or IrO_2),[69–74,189] which have an overpotential requirement not exceeding 150–200 mV under acidic conditions.[190] Nevertheless, the need to find economically viable materials and the inspiration from Mn_4CaO_x clusters of photosystem II in natural photosynthesis thrust the exploitation of O_2-evolution cocatalysts using more abundant elements.

In recent years, several cost-effective cocatalysts, such as CoO_x,[99,101,102,123,191] Co_3O_4,[122] Co-Pi,[106,192] MnO_x,[123] NiO_x,[123] FeO_x,[123] and $B_2O_{3-x}N_x$,[95] for the photocatalytic O_2-production have been exploited. Among them the Co-based cocatalysts have received much attention due to their outstanding performance for O_2 evolution. Very recently, Domen *et al.*[101] reported the loading of CoO_x on a porous single-crystalline $LaTiO_2N$ (LTON) by an impregnation method followed by NH_3 treatment and calcination in air. The existence of cobalt oxide on the surface of LTON was confirmed by the HRTEM image shown in Fig. 13a. The photocatalytic O_2-production rate of LTON was increased by more than 29 times in the presence of CoO_x, which is even higher than that of the optimized IrO_2/LTON (Fig. 13b). The optimized CoO_x/LTON showed a very high QE of 27.1 ± 2.6% at 440 nm, far exceeding the values reported for previous photocatalysts with a 600 nm absorption edge. To further investigate this unusual enhancement after loading CoO_x cocatalyst, PEC tests and time-resolved infrared absorption (TR-IR) measurements were

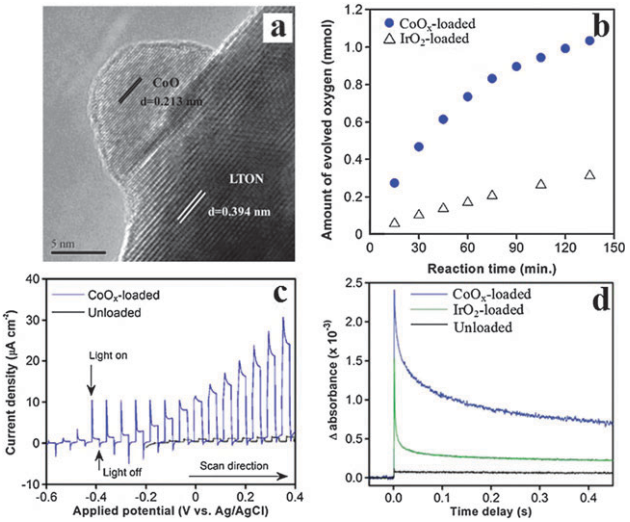

Fig. 13 (a) HRTEM image of a CoO_x/LTON sample. (b) Time course of O_2 evolution on LTON samples with different cocatalysts under visible-light irradiation (λ > 420 nm). (c) Photoanode currents of LTON electrodes with and without cobalt loading in 0.01 M Na_2SO_4 aqueous solution (pH 5.9). (d) Decay of photogenerated electrons on CoO_x-loaded LTON, IrO_2-loaded LTON and unloaded LTON. Reprinted with permission from ref. 101. Copyright 2012, American Chemical Society.

carried out. As shown in Fig. 13c, the CoO_x-modified LTON electrode generated much higher anodic photocurrent upon visible-light irradiation than that measured on an unmodified LTON electrode along with a more negative photocurrent onset potential, suggesting that CoO_x on LTON indeed promotes O_2 evolution. Besides, the deposition of CoO_x significantly increased the lifetime of carriers even to a time scale of 1 s (Fig. 13d). An exceptional O_2-evolution promotion effect of CoO_x together with the better separation of charge carriers explains the higher photocatalytic O_2-production activity of CoO_x/LTON. Moreover, one of the highest QE values in a wide-wavelength region (5.2% at 500–600 nm) for photocatalytic O_2 evolution was observed over Na_2CO_3 modified Ta_3N_5 after the loading of CoO_x cocatalyst.[102]

For non-oxide photocatalysts, it is of great importance to suppress their self-decomposition process caused by the photogenerated holes for achieving steady O_2 evolution.[48] The modification with CoO_x as an O_2 evolution promoter not only improved the photocatalytic activity of visible-light-responsive oxynitride Ga–Zn–In–O–N but also stabilized this system through extracting light-induced holes for water oxidation instead of self-oxidation.[191] Similarly, Wang *et al.*[122] found that the integration of Co_3O_4 NPs as a cocatalyst within g-C_3N_4 enhanced its activity and reliability.

It is widely accepted that the loading method of cocatalysts could not only determine the physicochemical properties of cocatalysts but also have an effect on the structure of base photocatalyst to some extent, thus greatly influencing the final photocatalytic activity. Therefore, the development of more effective loading methods to acquire beneficial properties of cocatalysts and base photocatalysts for achieving better activity is highly desirable. For instance, Li *et al.*[99] introduced a novel *in situ* sulfurization-assisted deposition method for loading

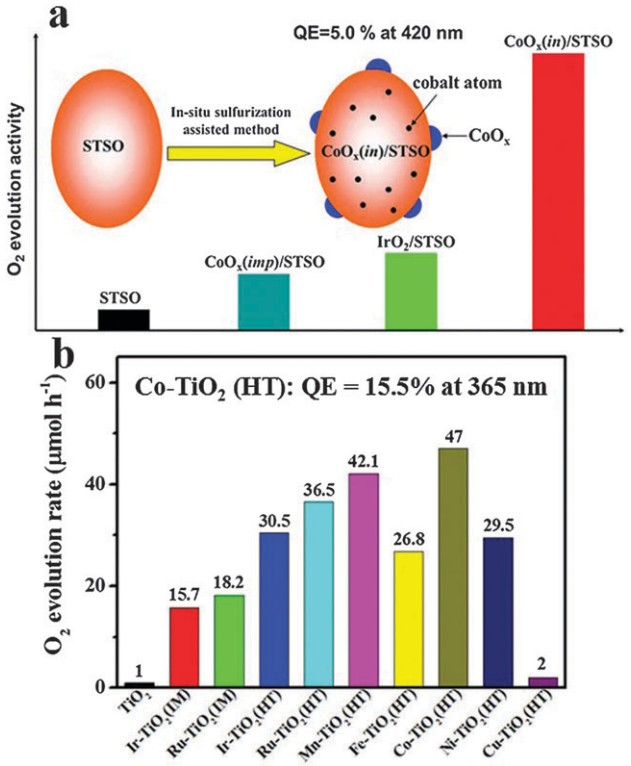

Fig. 14 (a) Schematic illustration of the *in situ* sulfurization-assisted deposition method for loading CoO_x cocatalyst on $Sm_2Ti_2S_2O_5$ (STSO) oxysulfide and a comparison of O_2-evolution activity of STSO, CoO_x/STSO obtained by impregnation, IrO_2-deposited STSO and CoO_x/STSO prepared by *in situ* sulfurization-assisted deposition. (b) Comparison of the O_2-evolution rate of different photocatalysts. Reprinted with permission from ref. 99 and 123. Copyright 2013, American Chemical Society.

CoO_x as a cocatalyst on $Sm_2Ti_2S_2O_5$ (STSO) oxysulfide. In comparison to traditionally impregnated cobalt or IrO_2 colloids, the sulfurization-assisted cobalt deposition well preserves the structure of photocatalysts and suppresses the formation of defect sites, resulting in better separation of photogenerated carriers and O_2 evolution activity (Fig. 14a). The QE of *in situ* cobalt oxide deposited $Sm_2Ti_2S_2O_5$ (CoO_x(in)/STSO) was 5.0% at 420 nm, which is the highest O_2 evolution efficiency for oxysulfides reported so far. In another case, the size of cocatalyst was optimized by a new loading method for achieving higher photocatalytic performance. Liu *et al.*[123] reported an *in situ* loading of a series of transition metal (TM) oxide clusters (MnO_x, FeO_x, CoO_x, NiO_x, CuO_x, RuO_2 and IrO_2) with ultra-small size (~2 nm) on TiO_2 nanosheets by hydrothermal reaction (denoted as TM–TiO_2(HT)). For the purpose of comparison, RuO_2 and IrO_2 loaded TiO_2 nanosheets were also synthesized by a traditional impregnation method (denoted as Ru–TiO_2 (IM) and Ir–TiO_2 (IM)), in which the size of RuO_2 and IrO_2 NPs was as large as 5 nm. As shown in Fig. 14b, Mn–TiO_2 (HT) and Co–TiO_2 (HT) exhibited the highest photocatalytic O_2-production activity, which is almost 3 times that of Ir–TiO_2 (IM). Moreover, the QE of Co–TiO_2 (HT) and Mn–TiO_2 (HT) were 15.5% and 13.9% at 365 nm, respectively, indicating their excellent O_2-evolution performance. Since the electronic structures of heterojunctions between metal oxide clusters and TiO_2 depend on the size of the clusters, the ultra-small size (~2 nm) of *in situ* loaded clusters is believed to greatly facilitate the interfacial charge transfer (IFCT), which is the key for reaching higher O_2-evolution efficiency. These results show that base metal oxide clusters particularly CoO_x with small sizes can be promising substitutes for noble-metal oxide (RuO_2 and IrO_2) cocatalysts in photocatalysis.

In addition to cobalt oxides, cobalt-oxide-phosphate (Co-Pi), another cobalt-based material, is one of the most popular O_2-evolution catalysts. Originally reported by Kanan and Nocera,[193–197] Co-Pi is an amorphous material containing Co(III) ions, oxide and phosphate, and requires an overpotential of only 0.41 V at pH 7 to oxidize water (measured at 1 mA cm^{-2}).[198] Co-Pi can also enhance the efficiency of O_2 evolution when coupled with semiconductor photocatalysts. For example, Xu *et al.*[192] reported the photochemical deposition of Co-Pi NPs on the surface of ZnO in a neutral phosphate buffer solution containing Co^{2+} ions. The enhanced activity for oxygen evolution was directly observed over Co-Pi loaded ZnO. The results suggest that Co-Pi plays the role of a cocatalyst, which can trap photogenerated holes, leading to the enhancement of electron and hole separation efficiency. Lee *et al.*[106] reported a scalable method to prepare the Co-Pi modified mesoporous graphitic-carbon-nitride (mpg-CN_x), for the photocatalytic O_2 evolution, which was remarkably enhanced (400 times faster as compared to that of the untreated mpg-CN_x) by Co-Pi in a pH 7 phosphate buffer containing Ag^+ or $Na_2S_2O_8$ as an electron scavenger.

Apart from the above transitional-metal based cocatalysts, a metal-free cocatalyst, $B_2O_{3-x}N_x$ clusters, has been studied for photocatalytic oxygen evolution on WO_3.[95] It was found that $B_2O_{3-x}N_x$ showed a more than 3 times stronger capability for promoting the oxygen evolution rate of WO_3 than B_2O_3. Although the transfer of photogenerated holes from WO_3 to $B_2O_{3-x}N_x$ clusters seems impossible from the viewpoint of the relative band-edge position of WO_3 and $B_2O_{3-x}N_x$, the electron-tunneling effect is believed to enable the diffusion of light-induced holes from WO_3 to the clusters for O_2 evolution, thanks to the ultra-small size of $B_2O_{3-x}N_x$ clusters (2–5 nm) (Table 3). Q10

The above studies have demonstrated that the loading of cocatalysts could substantially enhance the performance of semiconductor photocatalysts for O_2-evolution half reactions, which is the key step in photocatalytic overall water splitting. Nevertheless, as compared to the exploration of earth-abundant H_2-evolution cocatalysts, there is much less investigation on the earth-abundant O_2-evolution cocatalysts as well as their role in the thermodynamics and kinetics of multi-electron/multi-proton coupled O_2-evolution half reactions, which definitely deserve much more attention.

5. Earth-abundant cocatalysts for overall water splitting

Although many noble-metal-free cocatalysts have been developed for photocatalytic H_2 and O_2 evolution half reactions in the presence of sacrificial reagents, there remains room for the

Table 3 Earth-abundant cocatalysts for photocatalytic O_2-evolution half reactions

Photocatalyst	Cocatalyst	Loading method	Light source[a]	Reactant solution	O_2 evolution: Activity (μmol h^{-1} g^{-1})	O_2 evolution: Quantum efficiency (%)	Stability	Enhancement factor[b]	Ref. (year)
$Sm_2Ti_2S_2O_5$	CoO_x	*In situ* sulfurization-assisted deposition	λ > 420 nm (Xe)	$AgNO_3$	1630	5 (420 nm)	<4 h	16.3	99 (2013)
	IrO_2	Adsorption			460			4.6	
$LaTiO_2N$	CoO_x	Impregnation	λ > 420 nm (Xe)	$AgNO_3$	3680	27.1 (440 nm)	<2.5 h	29.4	101 (2012)
	IrO_2	Adsorption			850			6.8	
Ta_3N_5	CoO_x	Impregnation	800 > λ > 420 nm (Xe)	$AgNO_3$	4500	5.2 (500–600 nm)			102 (2012)
TiO_2	CoO_x	Hydrothermal	UV (L)	$NaIO_3$	470	15.5 (420 nm)	>5 h	47	123 (2013)
	MnO_x				421	13.9 (420 nm)		42	
	FeO_x				268			27	
	IrO_2				305			31	
	RuO_2				365			37	
g-C_3N_4	Co_3O_4	Coating	λ > 420 nm (Xe)	$AgNO_3$	502	1.1 (420 nm)	<11 h	9.0	122 (2012)
g-C_3N_4	Co-Pi	Photo-assisted deposition	λ > 400 nm (Xe)	$Na_2S_2O_8$	1012		<20 h	400	106 (2013)
ZnO	Co-Pi	Photochemical deposition	UV-Vis (Xe)	$AgNO_3$	1558		<3 h	4.3	192 (2012)
WO_3	$B_2O_{3-x}N_x$	Thermal oxidation-nitriding	λ > 400 nm (Xe)	$AgNO_3$	745		>3 h	9.6	95 (2013)

[a] Xe: xenon lamp, L: UV lamp. [b] Enhancement factor is calculated from the activity enhancement of photocatalysts loaded with the optimal amount of cocatalysts over photocatalysts without the loading of cocatalysts.

development of similar inexpensive cocatalysts for overall water splitting. Different from the cocatalysts applied in half reactions, cocatalysts employed in overall water splitting are required to selectively catalyze the H_2 or O_2 evolution while suppressing both the photoreduction of O_2 and water formation from H_2 and O_2. As a result, to date only a few earth-abundant cocatalysts have been proved to be effective in overall water splitting.

5.1 Loading H_2-evolution cocatalysts

Many research groups have focused on developing H_2-evolution cocatalysts for overall water splitting because a large number of photocatalysts, particularly oxides, lack surface H_2-evolution sites rather than O_2-evolution sites since their CB levels are not sufficiently negative for electrons to reduce water to produce H_2 without catalytic assistance whereas their VB levels are usually positive enough for holes to oxidize water and form O_2 even in the absence of cocatalyst.[41] As a consequence, introducing cocatalysts for H_2 production onto these photocatalysts could significantly raise their water-splitting activity. In 1980, Domen *et al.*[127] successfully loaded NiO_x as a cocatalyst onto the surface of $SrTiO_3$. They found that the state of the loaded cocatalyst strongly influenced the photocatalytic activity of $NiO_x/SrTiO_3$ for the decomposition of water vapor.[134] As illustrated in Fig. 15, the reduction–reoxidation pretreatment results in a Ni–NiO core–shell structure on the surface of $SrTiO_3$. After treatment $NiO_x/SrTiO_3$ becomes capable of catalyzing pure water splitting while neither $SrTiO_3$ nor Ni-metal-loaded $SrTiO_3$ showed any activity. This is because the NiO layer on Ni could effectively impede the back reaction of H_2 and O_2 recombination on Ni as well as the oxidation of Ni by water. This technique has been deemed as one of the most effective modification approaches to achieve pure-water splitting using particulate photocatalysts, even though the optimal modification conditions

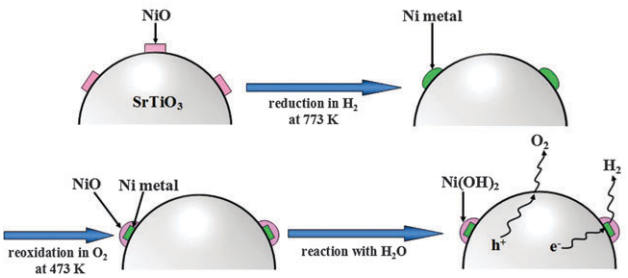

Fig. 15 Schematic view of the structures of a NiO–$SrTiO_3$ photocatalyst after various treatments. Reprinted with permission from ref. 134. Copyright 1986, American Chemical Society.

to some extent rely on the photocatalysts. So far, NiO_x has been successfully applied to many oxide semiconductor photocatalytic systems.[35,119,127–136,199–217]

Although NiO_x is a powerful cocatalyst capable of enormously enhancing the activity of numerous photocatalysts, many of which actually show no or negligible activity alone for pure water splitting, the overall photocatalytic efficiency achieved now is still far from satisfactory. In order to develop cocatalysts with higher activity and selectivity than NiO_x, the Domen group investigated the addition of another transition metal to NiO_x as a two-component cocatalyst to examine the enhancement effect. In 2000, they reported that both the photocatalytic activity and stability of Ni-loaded $K_2La_2Ti_3O_{10}$ for overall water splitting could be further enhanced *via* loading Cr by a co-impregnation method.[218] Based on this work, in 2006, they conducted a systematic study of co-loading Cr with various transition metals (*e.g.* Fe, Co, Ni, Cu, Ru, Rh, Pd, Ag, Ir and Pt) as a two-component cocatalyst on $(Ga_{1-x}Zn_x)(N_{1-x}O_x)$ for overall photocatalytic water splitting.[219] It was found that the

activity of $(Ga_{1-x}Zn_x)(N_{1-x}O_x)$ modified with different transition metals is remarkably improved by co-loading of Cr. Particularly, loading cocatalyst with a combination of 1 wt% Rh and 1.5 wt% Cr on reaction conditions. Furthermore, characterization results disclosed that the generation of trivalent Rh–Cr mixed oxide nanoparticles (10–30 nm in size) with optimal composition and distribution significantly improved the activity of $(Ga_{1-x}Zn_x)(N_{1-x}O_x)$.[220] To date, a QE of about 5.1% at 410 nm has already been obtained on the optimized $Rh_{2-y}Cr_yO_3/(Ga_{1-x}Zn_x)(N_{1-x}O_x)$,[221] which is at least an order of magnitude higher than that obtained with $RuO_2/(Ga_{1-x}Zn_x)(N_{1-x}O_x)$. The better activity of $Rh_{2-y}Cr_yO_3$ results from its superior capability for H_2-evolution together with its inactivity for the back reaction of O_2 photoreduction and water formation.[222] In addition, a new type of Rh–Cr_2O_3 (core–shell) cocatalyst has been developed and it also exhibited an excellent performance for assisted overall water splitting.[76] Both $Rh_{2-y}Cr_yO_3$ and Rh/Cr_2O_3 are proven to be generally active for other photocatalytic systems, such as $(Zn_{1+x}Ge)(N_2O_x)$ and GaN.[223,224]

$Rh_{2-y}Cr_yO_3$ and Rh/Cr_2O_3 are so far the most powerful cocatalysts for overall water splitting. Nevertheless, the high cost and rareness of noble-metal Rh seriously limit their massive application. In 2011, Domen *et al.*[225] developed a mixed oxide of Cu(II) and Cr(III) as a noble-metal-free cocatalyst for overall photocatalytic water splitting with a $(Ga_{1-x}Zn_x)(N_{1-x}O_x)$ solid solution. The activity of this photocatalyst was found to be greatly enhanced by the generation of Cu(II)–Cr(III) mixed-oxide NPs with optimal composition and coverage. Although the highest activity of $(Ga_{1-x}Zn_x)(N_{1-x}O_x)$ modified with a Cu(II)–Cr(III) mixed-oxide was at most 25–30% of that achieved using a similarly optimized photocatalyst loaded with $Rh_{2-y}Cr_yO_3$, the cost of Cu is about three orders of magnitude cheaper than that of Rh, which is beneficial for large-scale utilization. Domen groups have developed H_2-evolution cocatalysts with both excellent activity and selectivity for overall water splitting, such as the core–shell structured Ni–NiO and Rh–Cr_2O_3 as well as mixed oxides of CrO_x–NiO_y, $Rh_{2-y}Cr_yO_3$ and $CuCrO_x$, in which the NiO shell, the Cr_2O_3 shell or the CrO_x component plays the pivotal role of inhibiting O_2 photoreduction and water formation to improve the selectivity of cocatalysts for H_2 evolution.

Very recently, other groups reported novel types of H_2-evolution cocatalysts for overall water splitting, *e.g.* WC NPs and $[Mo_3S_4]^{4+}$ cluster. Takanabe *et al.*[121] have synthesized tungsten carbide NPs with a size of approximately 5 to 15 nm from the confinement of a mesoporous g-C_3N_4 template. Electrochemical measurements showed that WC phase with a large surface area exhibits both high activity and stability in HER while its activity in oxygen reduction reaction (ORR) is poor. Such a native selectivity makes WC a successful cocatalyst on Na-doped $SrTiO_3$ for overall water splitting. Different from the conventional nanoparticulate cocatalysts, a novel molecular cocatalyst $[Mo_3S_4]^{4+}$ cluster with an incomplete cubane-type structure (Fig. 16a) was loaded on $NaTaO_3$ by a facile impregnation method and a stoichiometric production of H_2 and O_2 was achieved.[96] The photocatalytic H_2-production rate in pure water over $NaTaO_3$ was increased by a factor of 28 *via* loading $[Mo_3S_4]^{4+}$ cluster as a cocatalyst (Fig. 16b). In comparison to the NP counterparts, these molecular units consist of only surface atoms/edge sites and thus have a large number of active sites for H_2 evolution. Such an advantage can be maximized with nanosized semiconductor photocatalysts. Therefore, molecular unit cocatalysts represent another important factor for highly efficient water splitting.

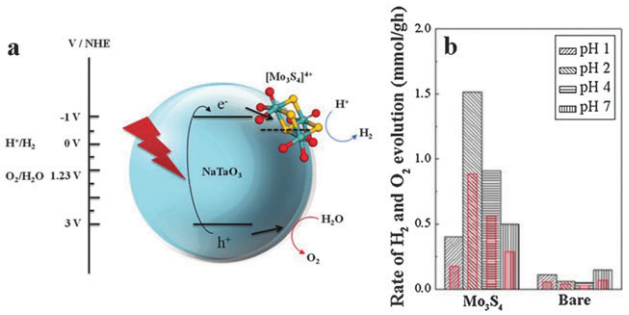

Fig. 16 (a) Schematic representation of $[Mo_3S_4]^{4+}$ loaded $NaTaO_3$ and the crystal structure of $[Mo_3S_4]^{4+}$ (S in yellow, Mo in green and O in red). One $[Mo_3S_4]^{4+}$ contains nine H_2O ligands. (b) pH dependent photocatalytic activity of $NaTaO_3$ with $[Mo_3S_4]^{4+}$ and the bare $NaTaO_3$ (black bar: H_2, red bar: O_2). Reprinted with permission from ref. 96. Copyright 2012, Royal Society of Chemistry.

5.2 Co-loading H_2- and O_2-evolution cocatalysts

As discussed above, significant efforts have been dedicated to developing cheap and efficient H_2-evolution cocatalysts. However, it would be natural to imagine that the water splitting activity would be further enhanced when both H_2 and O_2 evolution cocatalysts are loaded onto the same photocatalyst, in comparison to that of photocatalysts modified with either a H_2 or O_2 evolution cocatalyst alone. In 2010, Domen *et al.*[103] for the first time demonstrated the feasibility of modifying

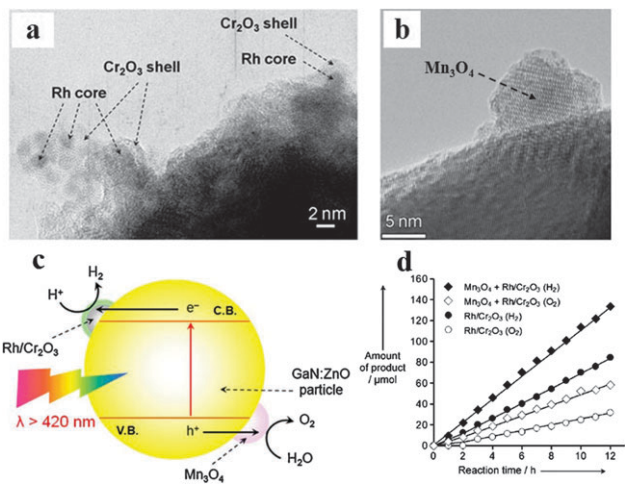

Fig. 17 TEM images of $(Ga_{1-x}Zn_x)(N_{1-x}O_x)$ modified with Mn_3O_4 and Rh–Cr_2O_3 (core–shell) nanoparticles: (a) Rh–Cr_2O_3. (b) Mn_3O_4. (c) A proposed reaction mechanism for visible-light-driven overall water splitting on $(Ga_{1-x}Zn_x)(N_{1-x}O_x)$ modified with Mn_3O_4 and Rh–Cr_2O_3 (core–shell) nanoparticles. C.B.: conduction band, V.B.: valence band, e^-: electron, h^+: hole. (d) Time course of H_2 and O_2 evolution using modified $(Ga_{1-x}Zn_x)(N_{1-x}O_x)$ photocatalysts under visible light ($\lambda > 420$ nm). Reprinted with permission from ref. 103. Copyright 2010, John Wiley & Sons, Inc.

Table 4 Earth-abundant cocatalysts for overall photocatalytic water splitting

Photocatalyst	Cocatalyst	Loading method	Light source[b]	Reactant solution	H_2 and O_2 evolution: Activity ($\mu mol\ h^{-1}\ g^{-1}$)	Quantum efficiency (%)	Stability	Enhancement factor[c]	Ref. (year)
$NaTaO_3$: La	NiO	Impregnation	UV-Vis (Hg)	Pure water	19 800 and 9660	56 (270 nm)	>390 h	44	119 (2003)
$La_4Ti_3O_{12}$	NiO	Impregnation	UV-Vis (Hg)	Pure water	714 and 358			40	129 (2009)
$CaLa_4Ti_4O_{15}$	NiO_x	Impregnation	UV-Vis (Hg)	Pure water	1186 and 552			198	129 (2009)
$SrLa_4Ti_4O_{15}$	NiO_x	Impregnation	UV-Vis (Hg)	Pure water	2342 and 1092			586	129 (2009)
$BaLa_4Ti_4O_{15}$	NiO_x	Impregnation	UV-Vis (Hg)	Pure water	4600 and 2308	15 (270 nm)	<4 h	460	129 (2009)
	RuO_2	Impregnation			1150 and 530			115	
$Ba_3LaNb_3O_{12}$	NiO_x	Impregnation	UV-Vis (Hg)	Pure water	2370 and 1176			593	129 (2009)
$Sr_5Nb_4O_{15}$	NiO_x	Impregnation	UV-Vis (Hg)	Pure water	4400 and 2200			733	129 (2009)
$Ba_5Nb_4O_{15}$	NiO_x	Impregnation	UV-Vis (Hg)	Pure water	8042 and 3944	17 (270 nm)		1340	129 (2009)
$Sr_2Nb_2O_7$	NiO_x	Impregnation	UV-Vis (Hg)	Pure water	402 and 198	23 (<300 nm)	>20 h	40	130 (2000)
$La_2Ti_2O_7$	NiO_x	Impregnation	UV-Vis (Hg)	Pure water	1376 and 670				131 (2002)
Ta_2O_5	NiO_x	Impregnation	UV-Vis (Hg)	Pure water	1030 and 544		>200 h	12.3	135 (2001)
Mg–Ta oxide	NiO_x	Impregnation	UV-Vis (Hg)	Pure water	340 and 170		>170 h	1.8	136 (2004)
$Sr_3Ti_2O_7$	NiO_x	Impregnation	λ < 400 nm (Hg)	Pure water	144 and ~72	4.3 (360 nm)	<120 h	206	199 (2006)
$RbNdTa_2O_7$	NiO_x	Impregnation	UV (Hg)	Pure water	586 and 293.5			2.5	200 (2000)
Ta_2O_5	NiO_x	Impregnation	λ > 200 nm (Hg)	Pure water	11 200 and 5433		<6 h		201 (2008)
$RbLaTa_2O_7$	NiO_x	Impregnation	UV (Hg)	Pure water	278 and 132			16.8	202 (2003)
$NaLaTa_2O_7$	NiO_x	Impregnation	UV (Hg)	Pure water	277 and 132			22.1	202 (2003)
$K_3Ta_3Si_2O_{13}$	NiO	Impregnation	UV-Vis (Hg)	Pure water	368 and 188			8.6	203 (2003)
$Sr_2Ta_2O_7$	NiO	Impregnation	UV-Vis (Hg)	Pure water	1000 and 480	12 (270 nm)		18.9	203 (2003)
La_3TaO_7	NiO_x	Impregnation	λ > 200 nm (Hg)	Pure water	328 and 164		>7 h	2.1	205 (2004)
$NaCa_2Ta_3O_{10}$	NiO_x	Impregnation	UV-Vis (Hg)	Pure water	1540 and 790	~5	>9 h		206 (2005)
$Y_2Ti_2O_7$	NiO_x	Impregnation	λ > 200 nm (Hg)	Pure water	1700 and 840				208 (2006)
$Gd_2Ti_2O_7$	NiO_x	Impregnation	λ > 200 nm (Hg)	Pure water	800 and 396				208 (2006)
$LaTaO_4$	NiO_x	Impregnation	UV-Vis (Hg)	Pure water	578 and 258			16.8	210 (2001)
$K_{1.15}Ta_{0.92}Zr_{0.08}O_3$	NiO_x	Impregnation	UV-Vis (Xe)	Pure water	122 and 57		<6 h		213 (1999)
$Sr_5Ta_4O_{15}$	NiO	Impregnation	UV-Vis (Hg)	Pure water	2388 and 1444		<6 h		215 (2005)
Lu_2O_3/Ga_2O_3: Zn	NiO_x	Impregnation	UV-Vis (Hg)	Pure water	100 and 53	6.81 (320 nm)	>200 h		216 (2004)
$K_2La_2Ti_3O_{10}$	NiO_x	Impregnation	λ > 190 nm (Hg)	KOH	507 and 253		<86 h		218 (2000)
	CrO_x–NiO_y	Coimpregnation			885 and 442		<124 h		
$(Ga_{1-x}Zn_x)(N_{1-x}O_x)$	CrO_x–NiO_y	Coimpregnation	λ > 300 nm (Hg)	Pure water	2283 and 1120		>5 h		219 (2006)
	CrO_x–CuO_y				1950 and 973		<25 h		
	CrO_x–RhO_y				12 783 and 6627				
$(Ga_{1-x}Zn_x)(N_{1-x}O_x)$	$CuCrO_x$	Coimpregnation	λ > 300 nm (Hg)	Pure water	2227 and 1140				225 (2011)
			λ > 400 nm (Hg)		167 and 83		>20 h		
$NaTaO_3$	$[Mo_3S_4]^{4+}$	Impregnation	UV-Vis (Hg)	Pure water	1700 and 850		<4 h	28	96 (2012)
g-C_3N_4	H_2–CoCat[a] and CoPi	*In situ* photo-reduction and chemical reduction and photo-assisted oxidation	λ > 400 nm (Xe)	Phosphate buffer	13.6 and 6.6		>15 h		106 (2013)

[a] H_2-CoCat: cobalt-oxo/hydroxo-phosphate compound from partially photoreduced Co-Pi. [b] Xe: xenon lamp, Hg: mercury lamp. [c] Enhancement factor is calculated from H_2-production activity enhancement of photocatalysts loaded with the optimal amount of cocatalysts over photocatalysts without the loading of cocatalysts.

$(Ga_{1-x}Zn_x)(N_{1-x}O_x)$ with core–shell-structured Rh–Cr_2O_3 and Mn_3O_4 NPs as H_2 and O_2 evolution promoters, respectively, to improve water splitting activity under visible light (Fig. 17a and b). As illustrated in Fig. 17c, the proposed reaction mechanism showed that Rh–Cr_2O_3 (core–shell) NPs functioned as H_2 evolution sites, while loaded Mn_3O_4 NPs accommodated O_2 evolution sites, as suggested by PEC measurements. With the aid of Mn_3O_4 NPs in promoting O_2 evolution, the photocatalytic activity for overall water splitting on $(Ga_{1-x}Zn_x)(N_{1-x}O_x)$ loaded with Rh–Cr_2O_3 (core–shell) NPs was further enhanced (Fig. 17d). Moreover, this co-loading method is also applicable to $SrTiO_3$, a metal oxide photocatalyst, suggesting the general utility of this method. A further study indicated that the overall-water splitting activity of $(Ga_{1-x}Zn_x)(N_{1-x}O_x)$ was more strongly influenced by the activity of H_2-evolution cocatalyst, though co-loading of O_2-evolution cocatalyst improved the photocatalytic efficiency to some extent.[226] This is because the surface of $(Ga_{1-x}Zn_x)(N_{1-x}O_x)$ lacks H_2-evolution sites rather than O_2-evolution sites, which is common for many photocatalysts. This study demonstrates that the development of more efficient H_2-evolution cocatalysts is a priority to further enhance the effect of co-loading method. Very recently, Domen *et al.*[104] for the first time reported that direct splitting of pure water into H_2 and O_2 could be achieved on a d^0-transition-metal-based oxynitride of ZrO_2-modified TaON under visible light. The dual loading of H_2 and O_2 evolution cocatalysts improved both the water splitting activity and stability of TaON. Lee *et al.*[106] showed that under visible-light illumination, the O_2-evolution cocatalyst Co-Pi loaded on mesoporous g-C_3N_4

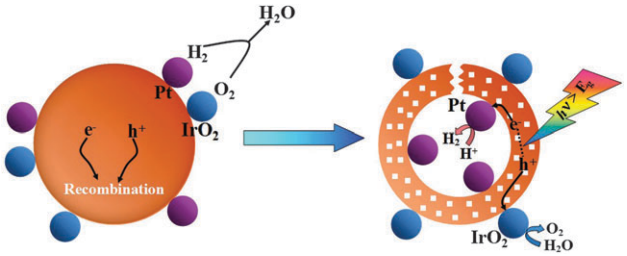

Fig. 18 Design principle, which involves the use of two spatially separated cocatalysts, Pt and IrO_2, on the core–shell Ta_3N_5 photocatalyst as effective charge collectors for water splitting. Reprinted with permission from ref. 105. Copyright 2013, John Wiley & Sons, Inc.

could be partly reduced by photogenerated electrons to form a cobalt-oxo/hydroxo-phosphate compound which acts as an efficient H_2-evolution cocatalyst (H_2-CoCat). Then the mesoporous g-C_3N_4 co-loaded with noble-metal-free Co-Pi and H_2-CoCat could produce a stoichiometric amount of H_2 and O_2 with rates of 13.6 μmol g^{-1} h^{-1} and 6.6 μmol g^{-1} h^{-1} in phosphate buffer at pH 7 without any electron–hole scavenger (Table 4).

Though the above models have successfully showed a great potential of co-loading method for improving the water splitting activity and stability of various photocatalysts, a full advantage of loading both reduction and oxidation sites, such as rectified charge separation, could not be demonstrated because the cocatalysts were usually deposited on the surface randomly. To resolve this problem, Domen *et al.*[105] presented a proof-of-concept using a SiO_2–Ta_3N_5 core–shell photocatalyst loaded with Pt NPs on the inner Ta_3N_5 shell surface as an electron collector and IrO_2 or CoO_x on the outer shell surface as a hole collector (see Fig. 18). As shown in Fig. 18, the spatially separated cocatalysts promote the separation and migration of photogenerated electrons and holes toward inner and outer surfaces, respectively, thereby inhibiting charge recombination as well as the backward reaction. Although only a few successful and reliable models utilizing the co-loading method have been reported till now[103,104,106,273] and noble-metal based cocatalysts are still needed to achieve reasonable activity, this dual loading method provides an important route to further improve the photocatalytic water-splitting performance using only earth-abundant cocatalysts in the future.

6. Conclusion and perspectives

In summary, highly active and robust cocatalysts composed of inexpensive and earth-abundant elements are indispensable for achieving high-efficiency, stable and cost-effective photocatalytic water splitting. In general, cocatalysts play comprehensive roles of (i) trapping charge carriers and inhibiting their recombination; (ii) accommodating H_2 and O_2 evolution sites and catalyzing gas evolution reactions by lowering activation energy; (iii) suppressing photo-corrosion of base photocatalysts. To date, a wide range of non-noble metal H_2-evolution cocatalysts have been successfully developed for photocatalytic H_2 production half reactions, which can be categorized into transition metals, transition metal compounds (*e.g.* oxides, hydroxides, sulfides and carbides), nanocarbons, nanocarbon-based composites, natural hydrogenases and artificial organometallic molecules. Among them, the highest QE reported is 51.3% at 420 nm for optimized NiS/CdS. In addition, it is noteworthy that the modification of CdSe nanocrystals with the molecular cocatalyst Ni–DHLA not only results in a very high QE (over 36% at 520 nm), but also produces a reportedly large TON (more than 600 000), implying a bright future for using artificial molecules as both highly efficient and stable cocatalysts. In contrast, only a handful of noble-metal-free O_2-evolution cocatalysts, such as Co_3O_4, CoO_x, MnO_x, FeO_x, NiO_x, $B_2O_{3-x}N_x$, and Co-Pi, have been reported for photocatalytic O_2 production half reactions. In particular, CoO_x-loaded $LaTiO_2N$ showed the highest QE of 27.1 ± 2.6% at 440 nm. In the case of pure water splitting, only NiO_x, $CuCrO_x$, WC and $[Mo_3S_4]^{4+}$ have been investigated as earth-abundant cocatalysts, mainly because cocatalysts utilized in overall water splitting should be resistant to both photoreduction of O_2 and water formation from H_2 and O_2. While the highest QE has reached 56% for NiO_x-loaded $NaTaO_3$:La under UV irradiation (λ = 270 nm), no appreciable QE for visible light has been reported for photocatalysts coupled with earth-abundant cocatalysts. Furthermore, co-loading H_2- and O_2-evolution cocatalysts offers a promising strategy to further enhance the photocatalytic activity of pure water splitting. Although some achievements have been made in developing low-cost cocatalysts, research on them is still at the primary stage, and there are many challenges towards significant improvement of photocatalytic water splitting efficiency and stability *via* modification with cocatalysts. Some issues are listed as follows:

(1) Fabrication and loading of earth-abundant cocatalysts:

The activity of a photocatalyst–cocatalyst composite is highly dependent on the fabrication and loading method of the cocatalyst, which determines the physicochemical properties of cocatalysts (such as chemical composition, phase structure, morphology, size distribution and surface area) as well as the interface/interaction between the cocatalyst and the base photocatalyst. Substantially enhanced photocatalytic activity would be expected by controlled synthesis of optimum-sized cocatalysts and their uniform dispersion on the surface of photocatalysts with an appropriate junction across the photocatalyst and the cocatalyst. Especially, it is very important to refine the loading conditions or develop more effective loading methods for the construction of atomically well-bonded nanojunctions, which would greatly facilitate the charge transfer due to the low or negligible energy barrier at the interface. Besides, such an intimate junction between the photocatalyst and the cocatalyst would bring another benefit of restraining the dissociation of the cocatalyst from the base photocatalyst during the photocatalytic process, thus increasing the lifetime of the photocatalyst–cocatalyst composite, which is one of the major challenges for its realistic application. Moreover, new methods for co-loading H_2 and O_2 evolution cocatalysts onto the same base photocatalyst should be developed, aiming to achieve spatially separated redox or gas-evolution active sites, which would maximize the effects of rectified electron–hole separation and avoid the recombination of H_2 and O_2. Furthermore, although most of the cocatalysts developed

now are one-component or core–shell-structured two-component nanoparticles, the constant appearance of novel photocatalysts and higher demand on the efficiency and durability of heterogeneous photocatalytic systems would inevitably drive the research and development of cocatalysts with multicomponent and/or new structures, which are unlikely to be acquired without advances in the fabrication and loading methods. Lastly, an ultimate goal of the massive energy production from water and sunlight using heterogeneous photocatalytic systems also requires a scalable, energy-saving and environmentally benign synthesis and loading method of cocatalysts on photocatalysts in the future.

(2) Development of novel earth-abundant cocatalysts with high activity, selectivity and stability for semiconductor-based photocatalytic water splitting:

The photocatalyst–cocatalyst composite system can be considered as a wireless microintegrated PEC cell, in which H_2 and O_2 evolution cocatalysts play the roles as water reduction and oxidation electrocatalysts, respectively. In fact, many electrocatalysts, such as NiS, $Ni(OH)_2$, MoS_2, MoS_3, WS_2, WC and Co-Pi, have already been proven to be highly efficient cocatalysts on semiconductors for photocatalytic water splitting. Therefore, it is reasonable to expect that the further development of novel earth-abundant cocatalysts can be inspired from developed inorganic and organometallic electrocatalysts. Inorganic electrocatalysts, such as binary or trinary metal alloys, mixed-metal oxides, spinels and perovskites, can be explored as cocatalysts. The synergetic effects reported in the multicomponent inorganic electrocatalysts could possibly lead to their high activity as cocatalysts in photocatalytic water splitting. Additionally, novel nanocarbon materials, especially graphene, can be combined with electrocatalysts to form a composite cocatalyst, in which the synergetic effect has been proven to greatly enhance the photocatalytic activity of coupled semiconductors. In regard to the overall water splitting, the selectivity of cocatalysts is the major concern. While seeking for a general and effective technique to suppress the back reactions on cocatalysts (such as co-loading CrO_x and coating Cr_2O_3 shell), the exploitation of cocatalysts with intrinsic selectivity like WC would be desirable. Furthermore, the durability of cocatalysts is a big challenge for their long-term performance on semiconductor photocatalysts. The pursuit of an effective strategy to inhibit the chemical- and/or photo-corrosion of cocatalysts should be favored. Organometallic molecules are another class of promising candidates to achieve potentially very high activity as cocatalysts due to their small dimension, which could introduce numerous active sites on nanosized photocatalysts. Besides, these molecules can be made from earth-abundant elements while offering the flexibility of tuning their properties by rational synthetic control of their structure. However, the poor water solubility and low stability are still two major problems for most of the organometallic molecules developed for catalyzing water reduction and oxidation. While connecting a water-soluble substituent to the molecules or directly incorporating these molecules in photocatalysts could enable their performance in purely aqueous solution, the long-term stability can possibly be realized *via* the design and synthesis of molecules which possess a bio-inspired self-healing function. Furthermore, few studies have been conducted on the use of molecular cocatalysts for overall photocatalytic water splitting, which is surely worthy of much more exploration.

(3) Fundamental studies on cocatalyst properties and functional mechanism:

The influence of various cocatalysts on the activity and stability of loaded semiconductor photocatalysts has been extensively investigated. However, the fundamental studies on the physicochemical properties, electrochemical performance, electron-transfer and multiple-electron coupled reaction mechanism of loaded cocatalysts are scarce and will be necessary to advance the field. In detail, a systematic study of the relationship between cocatalyst properties (*e.g.* chemical composition, phase structure, morphology, size distribution and surface area) and photocatalytic performance is required. Moreover, the electrochemical capabilities of cocatalysts for HER, oxygen evolution reaction (OER), ORR as well as H_2 and O_2 recombination should be explored to understand the origin of their activity and selectivity in photocatalytic water splitting. Furthermore, the nanoscale interface properties between photocatalysts and cocatalysts determine the eventual efficiency of the system. Thus, understanding the charge separation and transfer across the nanoscale interface is critical. In addition, the question of how multiple-electron reactions, particularly four-electron involved water oxidation, take place through cocatalysts has long been confusing to researchers and needs to be fully answered.

Acknowledgements

This work was financially supported by the Australian Research Council (ARC) through the Discovery Project programs (DP1095861 and DP130104459). Also this work was partially supported by the 973 program (2013CB632402) and NSFC (51320105001).

Notes and references

1 P. W. Du and R. Eisenberg, *Energy Environ. Sci.*, 2012, **5**, 6012.
2 J. C. Colmenares and R. Luque, *Chem. Soc. Rev.*, 2013, DOI: 10.1039/c3cs60262a. Q14
3 J. C. Colmenares, R. Luque, J. M. Campelo, F. Colmenares, Z. Karpiński and A. A. Romero, *Materials*, 2009, **2**, 2228.
4 Y. Q. Qu and X. F. Duan, *Chem. Soc. Rev.*, 2013, **42**, 2568.
5 A. Fujishima and K. Honda, *Nature*, 1972, **238**, 37.
6 E. Borgarello, J. Kiwi, M. Gratzel, E. Pelizzetti and M. Visca, *J. Am. Chem. Soc.*, 1982, **104**, 2996.
7 F. Zuo, L. Wang, T. Wu, Z. Zhang, D. Borchardt and P. Feng, *J. Am. Chem. Soc.*, 2010, **132**, 11856.
8 R. Niishiro, R. Konta, H. Kato, W. Chun, K. Asakura and A. Kudo, *J. Phys. Chem. C*, 2007, **111**, 17420.
9 R. Asahi, T. Morikawa, T. Ohwaki, K. Aoki and Y. Taga, *Science*, 2001, **293**, 269.
10 X. K. Li, N. Kikugawa and J. H. Ye, *Adv. Mater.*, 2008, **20**, 3816.

11 C. Z. Wen, Q. H. Hu, Y. N. Guo, X. Q. Gong, S. Z. Qiao and H. G. Yang, *Chem. Commun.*, 2011, **47**, 6138.
12 Q. Li, H. Meng, P. Zhou, Y. Q. Zheng, J. Wang, J. G. Yu and J. R. Gong, *ACS Catal.*, 2013, **3**, 882.
13 A. Kongkanand, K. Tvrdy, K. Takechi, M. Kuno and P. V. Kamat, *J. Am. Chem. Soc.*, 2008, **130**, 4007.
14 Z. Ning, H. Tian, C. Yuan, Y. Fu, H. Qin, L. Sun and H. Agren, *Chem. Commun.*, 2011, **47**, 1536.
15 Y. B. Chen and L. J. Guo, *J. Mater. Chem.*, 2012, **22**, 7507.
16 J. G. Yu, J. Zhang and M. Jaroniec, *Green Chem.*, 2010, **12**, 1611.
17 E. Borgarello, J. Kiwi, E. Pelizzetti, M. Visca and M. Gratzel, *Nature*, 1981, **289**, 158.
18 Y. I. Kim, S. Salim, M. J. Huq and T. E. Mallouk, *J. Am. Chem. Soc.*, 1991, **113**, 9561.
19 S. X. Min and G. X. Lu, *J. Phys. Chem. C*, 2011, **115**, 13938.
20 C. Gomes Silva, R. Juarez, T. Marino, R. Molinari and H. Garcia, *J. Am. Chem. Soc.*, 2011, **133**, 595.
21 E. Thimsen, F. Le Formal, M. Gratzel and S. C. Warren, *Nano Lett.*, 2011, **11**, 35.
22 T. Takahashi, A. Kudo, S. Kuwabata, A. Ishikawa, H. Ishihara, Y. Tsuboi and T. Torimoto, *J. Phys. Chem. C*, 2013, **117**, 2511.
23 X. Chen, L. Liu, P. Y. Yu and S. S. Mao, *Science*, 2011, **331**, 746.
24 G. Wang, H. Wang, Y. Ling, Y. Tang, X. Yang, R. C. Fitzmorris, C. Wang, J. Z. Zhang and Y. Li, *Nano Lett.*, 2011, **11**, 3026.
25 X. Wang, K. Maeda, A. Thomas, K. Takanabe, G. Xin, J. M. Carlsson, K. Domen and M. Antonietti, *Nat. Mater.*, 2008, **8**, 76.
26 Z. Yi, J. Ye, N. Kikugawa, T. Kako, S. Ouyang, H. Stuart-Williams, H. Yang, J. Cao, W. Luo, Z. Li, Y. Liu and R. L. Withers, *Nat. Mater.*, 2010, **9**, 559.
27 M. Sathish, B. Viswanathan and R. P. Viswanath, *Int. J. Hydrogen Energy*, 2006, **31**, 891.
28 N. Z. Bao, L. M. Shen, T. Takata and K. Domen, *Chem. Mater.*, 2008, **20**, 110.
29 N. Q. Wu, J. Wang, D. N. Tafen, H. Wang, J. Zheng, J. P. Lewis, X. G. Liu, S. S. Leonard and A. Manivannan, *J. Am. Chem. Soc.*, 2010, **132**, 6679.
30 H. B. Wu, H. H. Hng and X. W. Lou, *Adv. Mater.*, 2012, **24**, 2567.
31 J. G. Yu, Q. L. Li, J. J. Fan and B. Cheng, *Chem. Commun.*, 2011, **47**, 9161.
32 P. Madhusudan, J. R. Ran, J. Zhang, J. G. Yu and G. Liu, *Appl. Catal., B*, 2011, **110**, 286.
33 H. G. Yang, G. Liu, S. Z. Qiao, C. H. Sun, Y. G. Jin, S. C. Smith, J. Zou, H. M. Cheng and G. Q. M. Lu, *J. Am. Chem. Soc.*, 2009, **131**, 4078.
34 J. S. Chen, C. P. Chen, J. Liu, R. Xu, S. Z. Qiao and X. W. Lou, *Chem. Commun.*, 2011, **47**, 2631.
35 X. Wang, Q. Xu, M. R. Li, S. Shen, X. L. Wang, Y. C. Wang, Z. C. Feng, J. Y. Shi, H. X. Han and C. Li, *Angew. Chem., Int. Ed.*, 2012, **51**, 13089.
36 J. Lv, T. Kako, Z. S. Li, Z. G. Zou and J. H. Ye, *J. Phys. Chem. C*, 2010, **114**, 6157.
37 J. Zhang, S. Z. Qiao, L. F. Qi and J. G. Yu, *Phys. Chem. Chem. Phys.*, 2013, **15**, 12088.
38 F. Meng, J. T. Li, S. K. Cushing, M. J. Zhi and N. Q. Wu, *J. Am. Chem. Soc.*, 2013, **135**, 10286.
39 G. P. Dai, J. G. Yu and G. Liu, *J. Phys. Chem. C*, 2011, **115**, 7339.
40 X. B. Chen, S. H. Shen, L. J. Guo and S. S. Mao, *Chem. Rev.*, 2010, **110**, 6503.
41 A. Kudo and Y. Miseki, *Chem. Soc. Rev.*, 2009, **38**, 253.
42 H. L. Zhou, Y. Q. Qu, T. Zeida and X. F. Duan, *Energy Environ. Sci.*, 2012, **5**, 6732.
43 Y. Tachibana, L. Vayssieres and J. R. Durrant, *Nat. Photonics*, 2012, **6**, 511.
44 H. Tong, S. X. Ouyang, Y. P. Bi, N. Umezawa, M. Oshikiri and J. H. Ye, *Adv. Mater.*, 2012, **24**, 229.
45 Y. Zheng, J. Liu, J. Liang, M. Jaroniec and S. Z. Qiao, *Energy Environ. Sci.*, 2012, **5**, 6717.
46 A. Kubacka, M. Fernandez-García and G. Colon, *Chem. Rev.*, 2012, **112**, 1555.
47 M. Ni, M. K. H. Leung, D. Y. C. Leung and K. Sumathy, *Renewable Sustainable Energy Rev.*, 2007, **11**, 401.
48 K. Maeda and K. Domen, *J. Phys. Chem. C*, 2007, **111**, 7851.
49 F. E. Osterloh, *Chem. Mater.*, 2008, **20**, 35.
50 K. Zhang and L. Guo, *Catal. Sci. Technol.*, 2013, **3**, 1672.
51 K. Maeda, *J. Photochem. Photobiol., C*, 2011, **12**, 237.
52 I. Tsuji, H. Kato and A. Kudo, *Angew. Chem., Int. Ed.*, 2005, **44**, 3565.
53 M. Hara, J. Nunoshige, T. Takata, J. N. Kondo and K. Domen, *Chem. Commun.*, 2003, 3000.
54 Y. Sasaki, A. Iwase, H. Kato and A. Kudo, *J. Catal.*, 2008, **259**, 133.
55 K. Maeda, N. Sakamoto, T. Ikeda, H. Ohtsuka, A. Xiong, D. Lu, M. Kanehara, T. Teranishi and K. Domen, *Chem.–Eur. J.*, 2010, **16**, 7750.
56 F. N. Sayed, O. D. Jayakumar, R. Sasikala, R. M. Kadam, S. R. Bharadwaj, L. Kienle, U. Schurmann, S. Kaps, R. Adelung, J. P. Mittal and A. K. Tyagi, *J. Phys. Chem. C*, 2012, **116**, 12462.
57 J. G. Yu, L. F. Qi and M. Jaroniec, *J. Phys. Chem. C*, 2010, **114**, 13118.
58 S. R. Lingampalli, U. K. Gautam and C. N. R. Rao, *Energy Environ. Sci.*, 2013, **6**, 3589.
59 Q. Li, B. D. Guo, J. G. Yu, J. R. Ran, B. H. Zhang, H. J. Yan and J. R. Gong, *J. Am. Chem. Soc.*, 2011, **133**, 10878.
60 K. F. Wu, H. M. Zhu, Z. Liu, W. Rodriguez-Cordoba and T. Q. Lian, *J. Am. Chem. Soc.*, 2012, **134**, 10337.
61 H. J. Yan, G. J. Ma, G. P. Wu, X. Zong, Z. B. Lei, J. Y. Shi and C. Li, *J. Catal.*, 2009, **266**, 165.
62 Q. J. Xiang, J. G. Yu and M. Jaroniec, *J. Phys. Chem. C*, 2011, **115**, 7355.
63 K. Maeda, M. Higashi, D. L. Lu, R. Abe and K. Domen, *J. Am. Chem. Soc.*, 2010, **132**, 5858.
64 H. Y. Lin, H. C. Yang and W. L. Wang, *Catal. Today*, 2011, **174**, 106.
65 M. Murdoch, G. I. N. Waterhouse, M. A. Nadeem, J. B. Metson, M. A. Keane, R. F. Howe, J. Llorca and H. Idriss, *Nat. Chem.*, 2011, **3**, 489.

66 A. V. Korzhak, N. I. Ermokhina, A. L. Stroyuk, V. K. Bukhtiyarov, A. E. Raevskaya, V. I. Litvin, S. Y. Kuchmiy, V. G. Ilyin and P. A. Manorik, *J. Photochem. Photobiol., A*, 2008, **198**, 126.

67 S. Onsuratoom, T. Puangpetch and S. Chavadej, *Chem. Eng. J.*, 2011, **173**, 667.

68 J. H. Yang, D. Wang, H. X. Han and C. Li, *Acc. Chem. Res.*, 2013, **46**, 1900.

69 J. Sato, N. Saito, Y. Yamada, K. Maeda, T. Takata, J. N. Kondo, M. Hara, H. Kobayashi, K. Domen and Y. Inoue, *J. Am. Chem. Soc.*, 2005, **127**, 4150.

70 H. Liu, J. Yuan, W. Shangguan and Y. Teraoka, *J. Phys. Chem. C*, 2008, **112**, 8521.

71 K. Maeda, R. Abe and K. Domen, *J. Phys. Chem. C*, 2011, **115**, 3057.

72 W. J. Youngblood, S. H. A. Lee, Y. Kobayashi, E. A. Hernandez-Pagan, P. G. Hoertz, T. A. Moore, A. L. Moore, D. Gust and T. E. Mallouk, *J. Am. Chem. Soc.*, 2009, **131**, 926.

73 B. Ma, J. Yang, H. Han, J. Wang, X. Zhang and C. Li, *J. Phys. Chem. C*, 2010, **114**, 12818.

74 R. Abe, K. Shinmei, K. Hara and B. Ohtani, *Chem. Commun.*, 2009, 3577.

75 K. Maeda, K. Teramura, D. L. Lu, T. Takata, N. Saito, Y. Inoue and K. Domen, *Nature*, 2006, **440**, 295.

76 K. Maeda, K. Teramura, D. Lu, N. Saito, Y. Inoue and K. Domen, *Angew. Chem., Int. Ed.*, 2006, **45**, 7806.

77 J. G. Yu and J. R. Ran, *Energy Environ. Sci.*, 2011, **4**, 1364.

78 J. G. Yu, Y. Hai and B. Cheng, *J. Phys. Chem. C*, 2011, **115**, 4953.

79 J. R. Ran, J. G. Yu and M. Jaroniec, *Green Chem.*, 2011, **13**, 2708.

80 J. G. Yu, S. H. Wang, B. Cheng, Z. Lin and F. Huang, *Catal. Sci. Technol.*, 2013, **3**, 1782.

81 J. G. Yu, B. Yang and B. Cheng, *Nanoscale*, 2012, **4**, 2670.

82 T. Y. Peng, P. Zeng, D. N. Ke, X. J. Liu and X. H. Zhang, *Energy Fuels*, 2011, **25**, 2203.

83 J. Zhang, J. G. Yu, M. Jaroniec and J. R. Gong, *Nano Lett.*, 2012, **12**, 4584.

84 Q. J. Xiang, J. G. Yu and M. Jaroniec, *Nanoscale*, 2011, **3**, 3670.

85 J. Zhou, G. H. Tian, Y. J. Chen, X. Y. Meng, Y. H. Shi, X. R. Cao, K. Pan and H. G. Fu, *Chem. Commun.*, 2013, **49**, 2237.

86 W. Q. Fan, Q. H. Lai, Q. H. Zhang and Y. Wang, *J. Phys. Chem. C*, 2011, **115**, 10694.

87 Q. J. Xiang, J. G. Yu and M. Jaroniec, *J. Am. Chem. Soc.*, 2012, **134**, 6575.

88 K. A. Brown, S. Dayal, X. Ai, G. Rumbles and P. W. King, *J. Am. Chem. Soc.*, 2010, **132**, 9672.

89 K. A. Brown, M. B. Wilker, M. Boehm, G. Dukovic and P. W. King, *J. Am. Chem. Soc.*, 2012, **134**, 5627.

90 J. E. Huang, K. L. Mulfort, P. W. Du and L. X. Chen, *J. Am. Chem. Soc.*, 2012, **134**, 16472.

91 F. Wang, W. G. Wang, X. J. Wang, H. Y. Wang, C. H. Tung and L. Z. Wu, *Angew. Chem., Int. Ed.*, 2011, **50**, 3193.

92 C. B. Li, Z. J. Li, S. Yu, G. X. Wang, F. Wang, Q. Y. Meng, B. Chen, K. Feng, C. H. Tung and L. Z. Wu, *Energy Environ. Sci.*, 2013, **6**, 2597.

93 Z. J. Han, F. Qiu, R. Eisenberg, P. L. Holland and T. D. Krauss, *Science*, 2012, **338**, 1321.

94 Z. J. Li, J. J. Wang, X. B. Li, X. B. Fan, Q. Y. Meng, K. Feng, B. Chen, C. H. Tung and L. Z. Wu, *Adv. Mater.*, 2013, **25**, 6613.

95 Y. P. Xie, G. Liu, G. Q. Lu and H. M. Cheng, *Nanoscale*, 2012, **4**, 1267.

96 S. W. Seo, S. Park, H. Jeong, S. H. Kim, U. Sim, C. W. Lee, K. T. Nam and K. S. Hong, *Chem. Commun.*, 2012, **48**, 10452.

97 M. Tabata, K. Maeda, T. Ishihara, T. Minegishi, T. Takata and K. Domen, *J. Phys. Chem. C*, 2010, **114**, 11215.

98 F. Y. Wen, X. L. Wang, L. Huang, G. J. Ma, J. H. Yang and C. Li, *ChemSusChem*, 2012, **5**, 849.

99 R. G. Li, Z. Chen, W. Zhao, F. X. Zhang, K. Maeda, B. K. Huang, S. Shen, K. Domen and C. Li, *J. Phys. Chem. C*, 2013, **117**, 376.

100 Y. D. Hou, A. B. Laursen, J. S. Zhang, G. G. Zhang, Y. S. Zhu, X. C. Wang, S. Dahl and I. Chorkendorff, *Angew. Chem., Int. Ed.*, 2013, **52**, 3621.

101 F. Zhang, A. Yamakata, K. Maeda, Y. Moriya, T. Takata, J. Kubota, K. Teshima, S. Oishi and K. Domen, *J. Am. Chem. Soc.*, 2012, **134**, 8348.

102 S. S. K. Ma, T. Hisatomi, K. Maeda, Y. Moriya and K. Domen, *J. Am. Chem. Soc.*, 2012, **134**, 19993.

103 K. Maeda, A. Xiong, T. Yoshinaga, T. Ikeda, N. Sakamoto, T. Hisatomi, M. Takashima, D. L. Lu, M. Kanehara, T. Setoyama, T. Teranishi and K. Domen, *Angew. Chem., Int. Ed.*, 2010, **49**, 4096.

104 K. Maeda, D. L. Lu and K. Domen, *Chem.–Eur. J.*, 2013, **19**, 4986.

105 D. A. Wang, T. Hisatomi, T. Takata, C. S. Pan, M. Katayama, J. Kubota and K. Domen, *Angew. Chem., Int. Ed.*, 2013, **52**, 11252.

106 R. L. Lee, P. D. Tran, S. S. Pramana, S. Y. Chiam, Y. Ren, S. Y. Meng, L. H. Wong and J. Barber, *Catal. Sci. Technol.*, 2013, **3**, 1694.

107 A. K. Agegnehu, C. J. Pan, J. Rick, J. F. Lee, W. N. Su and B. J. Hwang, *J. Mater. Chem.*, 2012, **22**, 13849.

108 W. G. Wang, S. W. Liu, L. H. Nie, B. Cheng and J. G. Yu, *Phys. Chem. Chem. Phys.*, 2013, **15**, 12033.

109 Y. Yamada, T. Miyahigashi, H. Kotani, K. Ohkubo and S. Fukuzumi, *Energy Environ. Sci.*, 2012, **5**, 6111.

110 T. Sreethawong, Y. Suzuki and S. Yoshikawa, *Int. J. Hydrogen Energy*, 2005, **30**, 1053.

111 J. G. Yu, Y. Hai and M. Jaroniec, *J. Colloid Interface Sci.*, 2011, **357**, 223.

112 W. Zhang, Y. B. Wang, Z. Wang, Z. Y. Zhong and R. Xu, *Chem. Commun.*, 2010, **46**, 7631.

113 J. Zhang, J. G. Yu, Y. M. Zhang, Q. Li and J. R. Gong, *Nano Lett.*, 2011, **11**, 4774.

114 S. Xu, A. J. Du, J. Liu, J. Ng and D. D. Sun, *Int. J. Hydrogen Energy*, 2011, **36**, 6560.

115 D. P. Kumar, M. V. Shankar, M. M. Kumari, G. Sadanandam, B. Srinivas and V. Durgakumari, *Chem. Commun.*, 2013, **49**, 9443.

116 H. F. Dang, X. F. Dong, Y. C. Dong, Y. Zhang and S. Hampshire, *Int. J. Hydrogen Energy*, 2013, **38**, 2126.
117 H. Husin, W. Su, H. Chen, C. Pan, S. Chang, J. Rick, W. Chuang, H. Sheuc and B. Hwang, *Green Chem.*, 2011, **13**, 1745.
118 K. Shimizu, S. Itoh, T. Hatamachi, T. Kodama, M. Sato and K. Toda, *Chem. Mater.*, 2005, **17**, 5161.
119 H. Kato, K. Asakura and A. Kudo, *J. Am. Chem. Soc.*, 2003, **125**, 3082.
120 A. Kudo, K. Sayama, A. Tanaka, K. Asakura, K. Domen, K. Maruya and T. Onishi, *J. Catal.*, 1989, **120**, 337.
121 A. T. Garcia-Esparza, D. Cha, Y. W. Ou, J. Kubota, K. Domen and K. Takanabe, *ChemSusChem*, 2013, **6**, 168.
122 J. S. Zhang, M. Grzelczak, Y. D. Hou, K. Maeda, K. Domen, X. Z. Fu, M. Antonietti and X. C. Wang, *Chem. Sci.*, 2012, **3**, 443.
123 L. C. Liu, Z. Y. Li, W. X. Zou, X. R. Gu, Y. Deng, F. Gao, C. J. Tang and L. Dong, *ACS Catal.*, 2013, **3**, 2052.
124 P. D. Tran, L. F. Xi, S. K. Batabyal, L. H. Wong, J. Barber and J. S. C. Loo, *Phys. Chem. Chem. Phys.*, 2012, **14**, 11596.
125 C. Dinh, M. Pham, F. Kleitzb and T. Do, *J. Mater. Chem. A*, 2013, **1**, 13308.
126 N. Sakamoto, H. Ohtsuka, T. Ikeda, K. Maeda, D. Lu, M. Kanehara, K. Teramura, T. Teranishib and K. Domen, *Nanoscale*, 2009, **1**, 106.
127 K. Domen, S. Naito, M. Soma, T. Onishi and K. Tamaru, *J. Chem. Soc., Chem. Commun.*, 1980, 543.
128 C. Hu and H. S. Teng, *J. Catal.*, 2010, **272**, 1.
129 Y. Miseki, H. Kato and A. Kudo, *Energy Environ. Sci.*, 2009, **2**, 306.
130 D. W. Hwang, H. G. Kim, J. Kim, K. Y. Cha, Y. G. Kim and J. S. Lee, *J. Catal.*, 2000, **193**, 40.
131 J. Kim, D. W. Hwang, H. G. Kim, S. W. Bae, S. M. Ji and J. S. Lee, *Chem. Commun.*, 2002, 2488.
132 H. G. Kim, D. W. Hwang, J. Kim, Y. G. Kim and J. S. Lee, *Chem. Commun.*, 1999, 1077.
133 A. Kudo, A. Tanaka, K. Domen, K. Maruya, K. Aika and T. Onishi, *J. Catal.*, 1988, **111**, 67.
134 K. Domen, A. Kudo and T. Onish, *J. Phys. Chem.*, 1986, **90**, 292.
135 Y. Takahara, J. N. Kondo, T. Takata, D. L. Lu and K. Domen, *Chem. Mater.*, 2001, **13**, 1194.
136 J. N. Kondo, M. Uchida, K. Nakajima, D. Lu, M. Hara and K. Domen, *Chem. Mater.*, 2004, **16**, 4304.
137 Y. Ou, J. D. Lin, S. M. Fang and D. W. Liao, *Chem. Phys. Lett.*, 2006, **429**, 199.
138 L. Huang, X. L. Wang, J. H. Yang, G. Liu, J. F. Han and C. Li, *J. Phys. Chem. C*, 2013, **117**, 11584.
139 N. L. Wu and M. S. Lee, *Int. J. Hydrogen Energy*, 2004, **29**, 1601.
140 W. J. Foo, C. Zhang and G. W. Ho, *Nanoscale*, 2013, **5**, 759.
141 S. Fukuzumi and Y. Yamada, *ChemSusChem*, 2013, **6**, 1834.
142 M. K. Tian, W. F. Shangguan, J. Yuan, L. Jiang, M. X. Chen, J. W. Shi, Z. Y. Ouyang and S. J. Wang, *Appl. Catal., A*, 2006, **309**, 76.
143 J. Choi, S. Y. Ryu, W. Balcerski, T. K. Lee and M. R. Hoffmann, *J. Mater. Chem.*, 2008, **18**, 2371.
144 S. Y. Ryu, J. Choi, W. Balcerski, T. K. Lee and M. R. Hoffmann, *Ind. Eng. Chem. Res.*, 2007, **46**, 7476.
145 T. Sreethawong and S. Yoshikawa, *Catal. Commun.*, 2005, **6**, 661.
146 J. Bandara, C. P. K. Udawatta and C. S. K. Rajapakse, *Photochem. Photobiol. Sci.*, 2005, **4**, 857.
147 S. P. Xu and D. D. Sun, *Int. J. Hydrogen Energy*, 2009, **34**, 6096.
148 S. P. Xu, J. W. Ng, X. W. Zhang, H. W. Bai and D. D. Sun, *Int. J. Hydrogen Energy*, 2010, **35**, 5254.
149 S. S. Zhang, H. J. Wang, M. S. Yeung, Y. P. Fang, H. Yu and F. Peng, *Int. J. Hydrogen Energy*, 2013, **38**, 7241.
150 J. S. Jang, S. H. Choi, D. H. Kim, J. W. Jang, K. S. Lee and J. S. Lee, *J. Phys. Chem. C*, 2009, **113**, 8990.
151 T. S. Rocha, E. S. Nascimento, A. C. Silva, H. S. Oliveira, E. M. Garcia, L. C. A. Oliveira, D. S. Monteiro, M. Rodrigueza and M. C. Pereira, *RSC Adv.*, 2013, **3**, 20308.
152 H. Wender, R. V. Gonçalves, C. S. B. Dias, M. J. M. Zapata, L. F. Zagonel, E. C. Mendonça, S. R. Teixeirab and F. Garcia, *Nanoscale*, 2013, **5**, 9310.
153 J. Wang, B. Li, J. Z. Chen, N. Li, J. F. Zheng, J. H. Zhao and Z. P. Zhu, *Appl. Surf. Sci.*, 2012, **259**, 118.
154 J. D. Hong, Y. S. Wang, Y. B. Wang, W. Zhang and R. Xu, *ChemSusChem*, 2013, DOI: 10.1002/cssc.201300647.
155 L. Zhang, B. Z. Tian, F. Chen and J. L. Zhang, *Int. J. Hydrogen Energy*, 2012, **37**, 17060.
156 Y. P. Yuan, S. W. Cao, L. S. Yin, L. Xu and C. Xue, *Int. J. Hydrogen Energy*, 2013, **38**, 7218.
157 J. Zhang, Q. L. Xu, S. Z. Qiao and J. G. Yu, *ChemSusChem*, 2013, **6**, 2009.
158 L. J. Zhang, T. F. Jiang, S. Li, Y. C. Lu, L. L. Wang, X. Q. Zhang, D. J. Wang and T. F. Xie, *Dalton Trans.*, 2013, **42**, 12998.
159 X. Zong, H. J. Yan, G. P. Wu, G. J. Ma, F. Y. Wen, L. Wang and C. Li, *J. Am. Chem. Soc.*, 2008, **130**, 7176.
160 M. Nguyen, P. D. Tran, S. S. Pramana, R. L. Lee, S. K. Batabyal, N. Mathews, L. H. Wong and M. Graetzel, *Nanoscale*, 2013, **5**, 1479.
161 F. A. Frame and F. E. Osterloh, *J. Phys. Chem. C*, 2010, **114**, 10628.
162 M. L. Tang, D. C. Grauer, B. Lassalle-Kaiser, V. K. Yachandra, L. Amirav, J. Yano, J. R. Long and A. P. Alivisatos, *Angew. Chem., Int. Ed.*, 2011, **50**, 10203.
163 X. Zong, J. F. Han, G. J. Ma, H. J. Yan, G. P. Wu and C. Li, *J. Phys. Chem. C*, 2011, **115**, 12202.
164 J. Kibsgaard, Z. B. Chen, B. N. Reinecke and T. F. Jaramillo, *Nat. Mater.*, 2012, **11**, 963.
165 J. S. Jang, D. J. Ham, N. Lakshminarasimhan, W. Y. Choi and J. S. Lee, *Appl. Catal., A*, 2008, **346**, 149.
166 S. Iijima, *Nature*, 1991, **354**, 56.
167 L. L. Ma, H. Z. Sun, Y. G. Zhang, Y. L. Lin, J. T. Li, E. Wang, Y. Yu, M. Tan and J. B. Wang, *Nanotechnology*, 2008, **19**, 115709.

168 X. J. Liu, P. Zeng, T. Y. Peng, X. H. Zhang and K. J. Deng, *Int. J. Hydrogen Energy*, 2012, **37**, 1375.
169 K. S. Novoselov, A. K. Geim, S. V. Morozov, D. Jiang, Y. Zhang, S. V. Dubonos, I. V. Grigorieva and A. A. Firsov, *Science*, 2004, **306**, 666.
170 A. K. Geim and K. S. Novoselov, *Nat. Mater.*, 2007, **6**, 183.
171 Q. J. Xiang, J. G. Yu and M. Jaroniec, *Chem. Soc. Rev.*, 2012, **41**, 782.
172 Q. J. Xiang and J. G. Yu, *J. Phys. Chem. Lett.*, 2013, **4**, 753.
173 W. G. Tu, Y. Zhou and Z. G. Zou, *Adv. Funct. Mater.*, 2013, **23**, 4996.
174 G. C. Xie, K. Zhang, B. D. Guo, Q. Liu, L. Fang and J. R. Gong, *Adv. Mater.*, 2013, **25**, 3820.
175 A. H. Ye, W. Q. Fan, Q. H. Zhang, W. P. Deng and Y. Wang, *Catal. Sci. Technol.*, 2012, **2**, 969.
176 X. J. Lv, W. F. Fu, H. X. Chang, H. Zhang, J. S. Cheng, G. J. Zhang, Y. Song, C. Y. Hu and J. H. Li, *J. Mater. Chem.*, 2012, **22**, 1539.
177 T. Y. Peng, K. Li, P. Zeng, Q. G. Zhang and X. G. Zhang, *J. Phys. Chem. C*, 2012, **116**, 22720.
178 Z. Khan, T. R. Chetia, A. K. Vardhaman, D. Barpuzary, C. V. Sastri and M. Qureshi, *RSC Adv.*, 2012, **2**, 12122.
179 L. Jia, D. H. Wang, Y. X. Huang, A. W. Xu and H. Q. Yu, *J. Phys. Chem. C*, 2011, **115**, 11466.
180 B. Chai, T. Y. Peng, X. H. Zhang, J. Mao, K. Li and X. G. Zhang, *Dalton Trans.*, 2013, **42**, 3402.
181 S. X. Min and G. X. Lu, *J. Phys. Chem. C*, 2012, **116**, 25415.
182 X. J. Lv, S. X. Zhou, C. Zhang, H. X. Chang, Y. Chen and W. F. Fu, *J. Mater. Chem.*, 2012, **22**, 18542.
183 C. Tard and C. J. Pickett, *Chem. Rev.*, 2009, **109**, 2245.
184 F. Y. Wen, J. H. Yang, X. Zong, B. J. Ma, D. G. Wang and C. Li, *J. Catal.*, 2011, **281**, 318.
185 S. Cao, X. Liu, Y. Yuan, Z. Zhang, J. Fang, S. C. J. Loo, J. Barber, T. C. Sumb and C. Xue, *Phys. Chem. Chem. Phys.*, 2013, **15**, 18363.
186 J. F. Dong, M. Wang, X. Q. Li, L. Chen, Y. He and L. C. Sun, *ChemSusChem*, 2012, **5**, 2133.
187 S. S. K. Ma, K. Maeda, T. Hisatomi, M. Tabata and K. Domen, *Chem.–Eur. J.*, 2013, **19**, 7480.
188 A. Kasahara, K. Nukumizu, G. Hitoki, T. Takata, J. N. Kondo, M. Hara, H. Kobayashi and K. Domen, *J. Phys. Chem. A*, 2002, **106**, 6750.
189 B. H. Meekins and P. V. Kamat, *J. Phys. Chem. Lett.*, 2011, **2**, 2304.
190 V. Artero, M. Chavarot-Kerlidou and M. Fontecave, *Angew. Chem., Int. Ed.*, 2011, **50**, 7238.
191 K. Kamata, K. Maeda, D. Lu, Y. Kako and K. Domen, *Chem. Phys. Lett.*, 2009, **470**, 90.
192 Y. B. Wang, Y. S. Wang, R. R. Jiang and R. Xu, *Ind. Eng. Chem. Res.*, 2012, **51**, 9945.
193 M. W. Kanan and D. G. Nocera, *Science*, 2008, **321**, 1072.
194 M. W. Kanan, Y. Surendranath and D. G. Nocera, *Chem. Soc. Rev.*, 2009, **38**, 109.
195 Y. Surendranath, M. Dinca and D. G. Nocera, *J. Am. Chem. Soc.*, 2009, **131**, 2615.
196 D. A. Lutterman, Y. Surendranath and D. G. Nocera, *J. Am. Chem. Soc.*, 2009, **131**, 3838.
197 A. J. Esswein, Y. Surendranath, S. Y. Reece and D. G Nocera, *Energy Environ. Sci.*, 2011, **4**, 499.
198 F. E. Osterloh, *Chem. Soc. Rev.*, 2013, **42**, 2294.
199 H. Jeong, T. Kim, D. Kim and K. Kim, *Int. J. Hydrogen Energy*, 2006, **31**, 1142.
200 M. Machida, J. Yabunaka and T. Kijima, *Chem. Mater.*, 2000, **12**, 812.
201 Y. Noda, B. Lee, K. Domen and J. N. Kondo, *Chem. Mater.*, 2008, **20**, 5361.
202 M. Machida, K. Miyazaki, S. Matsushima and M. Arai, *J. Mater. Chem.*, 2003, **13**, 1433.
203 H. Kato and A. Kudo, *Catal. Today*, 2003, **78**, 561.
204 H. Kato and A. Kudo, *J. Phys. Chem. B*, 2001, **105**, 4285.
205 R. Abe, M. Higashi, Z. Zou, K. Sayama, Y. Abe and H. Arakawa, *J. Phys. Chem. B*, 2004, **108**, 811.
206 M. Machida, T. Mitsuyama, K. Ikeue, S. Matsushima and N. Arai, *J. Phys. Chem. B*, 2005, **109**, 7801.
207 M. Yoshino, M. Kakihana, W. S. Cho, H. Kato and A. Kudo, *Chem. Mater.*, 2002, **14**, 3369.
208 R. Abe, M. Higashi, K. Sayama, Y. Abe and H. Arakawa, *J. Phys. Chem. B*, 2006, **110**, 2219.
209 A. Kudo, H. Kato and S. Nakagawa, *J. Phys. Chem. B*, 2000, **104**, 571.
210 M. Machida, S. Murakami and T. Kijima, *J. Phys. Chem. B*, 2001, **105**, 3289.
211 D. W. Hwang, J. S. Lee, W. Li and S. H. Oh, *J. Phys. Chem. B*, 2003, **107**, 4963.
212 H. Kato and A. Kudo, *J. Photochem. Photobiol., A*, 2001, **145**, 129.
213 T. Ishihara, H. Nishiguchi, K. Fukamachi and Y. Takita, *J. Phys. Chem. B*, 1999, **103**, 1.
214 A. Kudo and H. Kato, *Chem. Phys. Lett.*, 2000, **331**, 373.
215 K. Yoshioka, V. Petrykin, M. Kakihana, H. Kato and A. Kudo, *J. Catal.*, 2005, **232**, 102.
216 D. Wang, Z. Zou and J. Ye, *Chem. Phys. Lett.*, 2004, **384**, 139.
217 T. K. Townsend, N. D. Browning and F. E. Osterloh, *Energy Environ. Sci.*, 2012, **5**, 9543.
218 C. T. K. Thaminimulla, T. Takata, M. Hara, J. N. Kondo and K. Domen, *J. Catal.*, 2000, **196**, 362.
219 K. Maeda, K. Teramura, N. Saito, Y. Inoue and K. Domen, *J. Catal.*, 2006, **243**, 303.
220 K. Maeda, K. Teramura, D. Lu, T. Takata, N. Saito, Y. Inoue and K. Domen, *J. Phys. Chem. B*, 2006, **110**, 13753.
221 K. Maeda and K. Domen, *J. Phys. Chem. Lett.*, 2010, **1**, 2655.
222 K. Maeda, K. Teramura, H. Masuda, T. Takata, N. Saito, Y. Inoue and K. Domen, *J. Phys. Chem. B*, 2006, **110**, 13107.
223 Y. Lee, K. Teramura, M. Hara and K. Domen, *Chem. Mater.*, 2007, **19**, 2120.
224 Y. Sakata, Y. Matsuda, T. Nakagawa, R. Yasunaga, H. Imamura and K. Teramura, *ChemSusChem*, 2011, **4**, 181.
225 K. Maeda, T. Ohnoa and K. Domen, *Chem. Sci.*, 2011, **2**, 1362.
226 A. Xiong, T. Yoshinag, T. Ikeda, M. Takashima, T. Hisatomi, K. Maeda, T. Setoyama, T. Teranishi and K. Domen, *Eur. J. Inorg. Chem.*, 2013, DOI: 10.1002/ejic.201300439.